The XDEM Multi-physics and Multi-scale Simulation Technology: Review on DEM-CFD Coupling, Methodology and Engineering Applications

Bernhard Peters, Maryam Baniasadi, Mehdi Baniasadi, Xavier Besseron, Alvaro Estupinan Donoso, Mohammad Mohseni, Gabriele Pozzetti

Université du Luxembourg, 6, rue Coudenhove-Kalergi, L-1359 Luxembourg

Abstract

The XDEM multi-physics and multi-scale simulation platform roots in the Extended Discrete Element Method (XDEM) and is being developed at the Institute of Computational Engineering at the University of Luxembourg. The platform is an advanced multi- physics simulation technology that combines flexibility and versatility to establish the next generation of multi-physics and multi-scale simulation tools. For this purpose the simulation framework relies on coupling various predictive tools based on both an Eulerian and Lagrangian approach. Eulerian approaches represent the wide field of continuum models while the Lagrange approach is perfectly suited to characterise discrete phases. Thus, continuum models include classical simulation tools such as Computational Fluid Dynamics (CFD) or Finite Element Analysis (FEA) while an extended configuration of the classical Discrete Element Method (DEM) addresses the discrete e.g. particulate phase. Apart from predicting the trajectories of individual particles, XDEM extends the application to estimating the thermodynamic state of each particle by advanced and optimised algorithms. The thermodynamic state may include temperature and species distributions due to chemical reaction and external heat sources. Hence, coupling these extended features with either CFD or FEA opens up a wide range of applications as di-

[1]Corrsponding author, bernhard.peters@uni.lu

verse as pharmaceutical industry e.g. drug production, agriculture food and processing industry, mining, construction and agricultural machinery, metals manufacturing, energy production and systems biology.

Keywords: multi-phase modelling, coupling CFD-DEM

1. Introduction

This section reviews major approaches in particular focussing on the combined approach of the Euler and Lagrange concept in a multi-phase flow context. For classical stand-alone concepts such as Computational Fluid Dynamics (CFD) or Finite Element Analysis (FEA) the reader is refereed to standard text books [1, 2, 3, 4].

Numerical approaches to model multi-phase flow phenomena including a solid e.g. particulate phase may basically be classified into two categories: All phases are treated as a continuum on a macroscopic level of which the two fluid model is the most well-known representative [5]. It is well suited to process modelling due to its computational convenience and efficiency. However, all the data concerning size distribution, shape or material properties of individual particles is lost to a large extent due to the averaging concept. Therefore, this loss of information on small scales has to be compensated for by additional constitutive or closure relations. Packed beds are frequently employed in engineering applications such as for thermal conversion of solid fuels e.g. biomass [6, 7] or blast furnaces for metallurgical processes [8]. Common to these engineering applications is a complex interaction of processes consisting of flow of a solid, liquid and gas phase with heat, mass and momentum transfer between them and including chemical conversion.

In the following sections numerical approaches to represent multiphase flow as gas-liquid, gas-powder and solid-fluid configurations are reviewed. It is followed by the technological concept of the XDEM suite and concludes with relevant and validated applications.

1.1. Gas-Liquid Multi-phase Flow

A potential flow model to describe the gas-liquid flow were employed by Szekely et al. [9], Sugiyama et al. [10] and Austin [11]. Another category of models is based on probability and statistical methods as employed by Ohno et al. [12], Wang et al. [13, 14] and Liu et al. [15]. The velocity of the liquid phase is determined stochastically in conjunction with a distribution function. Eto et al. [16] employed a tube-network dynamic model for simulation of the liquid flow in the dripping zone of a blast furnace.

Wang et al. [17] coupled continuum and probability approaches to describe the gas-liquid flow in packed beds. Within a continuum approach based on Darcy's equation the gas-liquid velocity is predicted by solving the coupled continuity and momentum equations as carried out by Takahashi et al. [18], Takahashi et al. [19], Kuwabara et al. [20], Chen et al. [21], Takatani et al. [22], Szekely et al. [9], Kajiwara et al. [23], Yagi et al. [24], Castro et al. [25], Sugiyama et al. [26], Zhang et al. [27], Austin et al. [28], Zaimi et al. [29], Castro et al. [30, 31], Eto et al. [16] and Chu et al. [32]. Due to the continuum approach detailed information on the structure of the packed bed is lost, that could be recovered by a fine grid taking into account the morphology such as porosity and was undertaken by Li et al. [33] and Wen et al. [34]. However, resolving the structure requires high CPU times, which was addressed by Wang et al. [35] and Wang et al. [13]. Wang et al. [35, 36] developed a model for which the numerical grid must not correspond to the structure of the packed bed e.g. size of the particles. Motion of the liquid phase is described by conservation equations for mass and momentum in two dimensions. The model was validated by data of Sugiyama [26] and yielded reasonable good agreement.

Based on their recent model developments [27], Zhang et al. [37] simulated the flow of solids in a blast furnace because the layered burden and consumption of solids effects the flow of gases in a blast furnaces as pointed out by Takahashi et al. [38]. Increasing the consumption rate of the solids reduces the size of the stagnant zone.

Das et al. [39] applied a continuous model to predict silicon transport in

the dripping zone of a blast furnace. They distinguished two mechanisms for hold-up for the liquid in the dripping zone through a multi-physics coupling of the heat transfer, liquid flow, species transport and chemical kinetics processes: Hold-up in the absence of gas flow and in the presence of counter current gas flow. Owing to the complexity of liquid hold- up, they applied a semi-empirical approach [40, 41, 42] including both static and dynamic components. They concluded that the counter current gas flow has no significant effect on the liquid hold-up under a stable blast furnace operating conditions.

Jin et al. [43, 44] described dripping of liquid metal through a packed bed taking into account counter-current flow and reactions between gas, solid and liquid phases. The latter were described by differential conservation equations for mass, momentum and energy and solved with COMSOL Multiphysics 3.4. The predicted results include both dynamic and static hold-up of liquid and showed the dependence of the temperature distribution due to endothermic reduction of silica.

Danloy et al. [45] developed a modular model to describe the performance of a blast furnace under steady state conditions. The modules incorporated represent a burden distribution according to Hamilius [46], flow of gases, liquids and solids including heat transfer between the phases and a cohesive zone sub-model. The flow of gases, liquids and solids is based on differential conservation equations. The cohesive zone sub-model starts at a solid temperature of 1200 °C and ends where ore is liquid accompanied by a set of five reactions for reduction of ore. After validation with vertical probe measurements of the blast furnace B at Sidmar, they predicted the influence of operating parameters such as burden distribution on gas distribution, pressure drop, productivity, shape and position of the cohesive zone and top gas temperature profile. Nogami et al. [47] undertook a numerical analysis of the blast furnace performance with novel feed material as carbon composite agglomerates (CCB). Their multi-fluid approach included reduction kinetics for ore [48, 8, 49, 50] and silicon [51, 52, 53]. Additional charging of carbon composite agglomerates lowered melting and hot metal temperatures, that contributes to an improved efficiency of the blast

furnace.

Yu et al. [54] also modelled the gas-liquid flow by a continuous approach in conjunction with a force balance approach and stochastic treatment of the packed bed structure. Good agreement between measurements and predictions allowed studying localised liquid flow and the effect of the cohesive zone on the gas flow.

However, experimental observations [55, 56, 57, 15, 58, 59, 13, 14, 41, 60, 24, 61] show that an above-mentioned pure continuous approach is inaccurate to represent the flow of discrete rivulets or droplets [62] for the configurations addressed. Therefore, a discrete approach seems to be more appropriate that describes the trajectories of individual liquid droplets or solid particles under the influence of gas drag forces, resistance from the solid phase possibly including its properties and gravity acting on discrete particles. Ohno and Schneider [12] were the first to represent liquid flow as spherical droplets moving through the porous space of a packed bed. Gupta et al. [56, 57] applied a balance of all major forces acting on a liquid mass to model liquid flow in a packed bed and has been used by Liu et al. [15] and Wang et al. [13, 14, 41, 63]. Xu et al. [64] and Chew et al. [65, 66, 67] also investigated into the discrete behaviour of the fluid phase. Singh and Gupta [68] investigated into the non-wetting liquid flow from a point source in a packed by a discrete model.

These models lack dispersion of the fluid phase, that is compensated by the statistical approaches of by Wang et al. [13, 14] and Liu et al. [15] to some extent. Chew et al. [69] reported from their experimental study that a flow pattern including horizontal and even upward flow exists.

Within a discrete approach both size and shape of liquid masses have to be determined for which various studies have been carried out [70, 71, 72, 73, 74, 75, 76]. However, due to the complexity to determine the shape Singh and Gupta [68] assumed a spherical shape for sufficiently large pore spaces and a rivulet otherwise. While the gas flow was described as a turbulent flow with the $k-\epsilon$-model, a global force balance determined the flow of droplets. Their approach was validated by measurements in a uniformly packed bed and agreement was

reported to be reasonable good.

1.2. Gas-Solid Multi-phase Flow

Gas-Solid multi-phase flow is distinguished by the size of the particulate flow. For very small sizes of the particles it is classified as powder while larger particle dimensions lead to the domain of packed, bubbling or fluidised beds. Hence, the following sections review individually these two multi-phase flow regimes.

1.2.1. Gas-Powder Flow

Fines may be entrained by ascending gas (dynamic holdup) whereas remaining fines are caught in the packed bed (static holdup). Hence, the fines effect the gas flow to a large extent as pointed out by Shibata et al. [77] and Chen et al. [78]. Shibata et al. [77] observed that static powder hold-up as a blockage takes place for gas velocities lower than a critical value that corresponds well with the transport velocity of one-dimensional models. Their model took into account convective transport, however, neglected viscous stress and body forces and was employed by Austin et al. [79, 80], Castro et al. [81] and Nogami et al. [82]. Chen et al. [78] extended the model of Shibata et al. [77] by static and dynamic powder hold-up. Pintowantoro et al. [83] investigated the static hold-up as proposed by Hikado et al. [84]. These findings were enhanced by modelling the effect of impermeable obstacles in the flow and powder accumulation in a packed bed by Dong et al. [85]. The strong influence of permeability on the gas-liquid flow was also emphasised by Horio [86]. They employed the continuous two-fluid approach that has been successfully applied by Jackson [87], Soo [88], Garg et al. [89], Gidaspow et al. [90], Kuipers et al. [91] and Levy [92]. They concluded that differences in physical properties determine the flow behaviour to a large extent including the dependency of dust accumulation on gas velocity, powder diameter and shape. The latter and its effect on gas-powder flow in a blast furnace in particular was investigated by Dong et al. [93]. They identified numerically powder hold-up regions in the central part of a blast furnace and lower part of the cohesive zone. Sugiyama et al. [94] analysed accumula-

tion in the deadman and dripping zone of blast furnace through experimental investigation of a two-phase flow through a parallel packed bed.

Yamaoka [95] reported that these regions of blockage also occur in two- or three-dimensional packed beds. He proposed a simple model for which the collision between fines and the particles of the packed bed dominate the behaviour. These findings were confirmed by Ichida et al. [96] who observed that fines were deposited near walls due to low gas velocities. Similarly, Yamaoka [97] found that dust may stick to particle surfaces close to injection, and thus reducing the outflow, however, not caused by low velocities.

In order to contribute to clarification of these phenomena observed Hidaka et al. [98] investigated experimentally into the entrainment of fine particles in a packed bed with a counter-current gas flow. Both dynamic and static hold-up were correlated with empirical equations. Furthermore, the pressure drop for a gas flow with entrained fines was slightly higher than for a pure gas flow. Similar experiments were carried out by Dong et al. [85] and they found that accumulation regions increase with high dust rates and low velocities. Furthermore, the structure of a packed bed in particular impermeable blocks in a packed bed promote accumulation of fines. The existence of impermeable fused layers was also confirmed by Steiler et al. [99]. This phenomenon of impermeable fused layers was investigated numerically by Wang et al. [63]. Their results indicate that a complex and non-uniform flow with horizontal and even upward flow takes place in the cohesive zone and in front of the raceways. Furthermore, liquids penetrating the void space in the coke layers leads to an increased hold-up.

Yagi [24] investigated the flow of four phases namely gas, liquid, solids and fines by differential conservation equations. Four phase flow was also addressed by Dong et al. [100]. They found that motion and structure of the solids effects the powder and liquid holdup to a large extent. Thus, they predicted a solid stagnant zone with a hold-up region for powder and liquid. They also stressed the fact that a flow model has to be coupled to a heat transfer and a chemical conversion model. Similar investigations were carried out by Aoki et al. [101] who predicted the behaviour of fine particles in the vicinity of the injection area.

In the injection region Yuu et al. [102] predicted stable and unstable flows and was carried out similarly by Takeda and Lockwood [103, 104].

1.2.2. Gas-Solid Flow

An alternative approach considers the solid phase as discrete, while the flow of liquids or gases is treated as a continuum phase in the void space between the particles, and therefore, is labelled the Combined Continuum and Discrete Model (CCDM) [105, 106, 107, 108]. Due to a discrete description of the solid phase, constitutive relations are omitted, and therefore, leads to a better understanding of the fundamentals. This was also concluded by Zhu et al. [109] and Zhu et al. [110] during a review on particulate flows modelled with the CCDM approach. It has seen a major development in last two decades and describes motion of the solid phase by the Discrete Element Method (DEM) on an individual particle scale and the remaining phases are treated by the Navier-Stokes equations. Thus, the method is recognized as an effective tool to investigate into the interaction between a particulate and fluid phase as reviewed by Yu and Xu [111], Feng and Yu [112] and Deen et al. [113].

Within a major review on particulate flows modelled with the CCDM approach Zhu et al. [109] and Zhu et al. [110] concluded that the methodology is well suited to understand the fundamental physics of these flows. However, current models including software should be extended to multi-phase flow behaviour and to particle shapes other than spherical geometries to meet engineering needs. These efforts should lead to a general link between continuum and discrete approaches so that results are quantified for process modelling.

Initially, such studies are limited to simple flow configurations [106, 105], however, Chu and Yu [114] demonstrated that the method could be applied to a complex flow configuration consisting of a fluidised bed, conveyor belt and a cyclone. Similarly, Zhou et al. [115] applied the CCDM approach to the complex geometry of fuel-rich/lean burner for pulverised coal combustion in a plant and Chu et al. [116] modelled the complex flow of air, water, coal and magnetite particles of different sizes in a dense medium cyclone (DMC). For both cases

remarkably good agreement between experimental data and predictions was achieved.

The CCDM approach has also been applied to fluidised beds as reviewed by Rowe and Nienow [117] and Feng and Yu [112] and applied by Feng and Yu [118] to the chaotic motion of particles of different sizes in a gas fluidised bed. Kafuia et al. [119] describe discrete particle-continuum fluid modelling of gas-solid fluidised beds.

A similar development has been seen for modelling of blast furnaces. Computational Fluid Dynamics (CFD) as a tool for continuous flow modelling has been applied with success to a large extend as reviewed by Chattopahyay et al. [120, 121]. The flow of the solid phase consisting of particles is to be modelled by a discrete approach as suggested by Dong et al. [122] and reviewed by Yu [123] for several engineering applications. Simsek et al. [124] predicted grate firing systems by the CCDM method, but obtained only qualitatively reasonable results highlighting the fact that more research is required.

However, current CCDM approaches should be extended to a truly multiphase flow behaviour as opposed to the Volume-of-Fluid method and the multiphase mixture model [125]. Furthermore, particle shapes other than spherical geometries have to be taken into account to meet engineering needs according to Zhu et al. [109] and Zhu et al. [110]. These efforts should ideally be complemented by poly-disperse particle systems since all derivations have done for mono-sized particles as stated by Feng and Yu [112]. All these efforts should contribute to a general link between continuum and discrete approaches so that results are quantified for process modelling.

Although the CCDM methodology has been established over the past decade [105, 107], prediction of heat transfer is still in its infancy. Kaneko et al. [126] predicted heat transfer for polymerisation reactions in gas-fluidised beds by the Ranz-Marshall correlation [127], however, excluding conduction. Swasdisevi et al. [128] predicted heat transfer in a two- dimensional spouted bed by convective transfer solely. Conduction between particles as a mode of heat transfer was considered by Li and Mason [129, 130, 131] for gas-solid transport in horizon-

tal pipes. Zhou et al. [132, 133] modelled coal combustion in a gas-fluidised bed including both convective and conductive heat transfer. Although, Wang et al. [134] used the two fluid model to predict the gas-solid flow in a high-density circulating fluidised bed, Malone and Xu [135] predicted heat transfer in liquid-fluidised beds by the CCDM method and stressed the fact that deeper investigations into heat transfer is required.

Although Xiang [136] investigated into the effect of air on the packing structure of fine particles, it is not feasible for large structures due to limited computational resources. A recent review of Zhou et al. [109] shows that a lot of approaches concentrate on flow solely without heat or mass transfer. They anticipate that future requirements will have to concentrate on the following issues [109]:

- "Microscale: To develop a more comprehensive theory and experimental techniques to study and quantify the interaction forces between particles, and between particle and fluid under various conditions, generating a more concrete basis for particle scale simulation." [109]

- "Macroscale: To develop a general theory to link the discrete and continuum approaches, so that particle scale information, generated from DEM or DEM-based simulation, can be quantified in terms of (macroscopic) governing equations, constitutive relations and boundary conditions that can be implemented in continuum-based process modelling." [109]

- "Application: To develop more robust models and efficient computer codes so that the capability of particle scale simulation can be extended, say, from two-phase to multiphase and/or from simple spherical to complicated non-spherical particle system, which is important to transfer the present phenomenon simulation to process simulation and hence meet real engineering needs." [109]

These findings are confirmed by Yu and Xu [111] who see the difficulties more associated with the solid phase than to the fluid phase. Hence, a coupling be-

tween DEM and CFD is more promissing due to its computational convenience than DNS- or LB-DEM interfaces. Yu and Xu [111], Zhu et al. [110] and Zhu et al. [109] gave a major review on particulate flows modelled with the CCDM approach and concluded that it is well suited to understand the fundamental physics of these flows.

1.3. Chemical Reaction, Heat and Mass Transfer

The theoretical foundation for the Extended Discrete Element Method (XDEM) was developed in 1999 by [137], who described incineration of a wooden moving bed on a forward acting grate [138] for which the particulate phase was resolved by an individual model describing various conversion processes. The concept was later also employed by [124] to predict the furnace process of a grate firing system.

Initial efforts within an Euler-Lagrange framework including the thermodynamic state of the particulate phase were proposed by Peters [138], This approach is also reffered to as the Combined Continuum and Discrete Model (CCDM) of which major reviews are found in Zhu et al. [109], Zhu et al. [110] Yu and Xu [111], Feng and Yu [112] and Deen et al. [113].

Exchange of heat mass, and momentum between the particulate and a fluid phase are described by empirical correlations as applied by Miltner et al. [20] for baled biomass. Similarly, Mehrabian et al. [139] and Gomez et al. [140] employed this approach for packed bed combustion. Thermal conversion of solid fuels on a forward acting grate were investigated through a coupling of CFD/DEM by Simsek et al. [124]. Wiese et al. [141] also predicted the performance of a pellet stove by CFD/DEM coupling and employing reduced order modelling for the particulate phase. However, no details on the ROM approach were provided. Further investigations with the coupled CFD/DEM technique within the same research group include a variety of applications such as drying in a rotary kiln [142, 143], municipal solid waste incineration [144], heat transfer [145] and calcination [146]. Kloos et al. [147] developed a CFD/DEM by coupling the open-source codes Lammps and OpenFoam to analyse heat transfer

in fluidised beds [148]. Kaneko et al. [126] predicted heat transfer for polymerisation reactions in gas-fluidised beds by the Ranz-Marshall correlation [127], however, excluding conduction. Swasdisevi et al. [128] predicted heat transfer in a two- dimensional spouted bed by convective transfer solely. Conduction between particles as a mode of heat transfer was considered by Li and Mason [129, 130, 131] for gas-solid transport in horizontal pipes. Zhou et al. [132, 133] modelled coal combustion in a gas-fluidised bed including both convective and conductive heat transfer. Although, Wang et al. [134] used the two fluid model to predict the gas-solid flow in a high-density circulating fluidised bed, Malone and Xu [135] predicted heat transfer in liquid-fluidised beds by the CCDM method and stressed the fact that deeper investigations into heat transfer is required. However, fluidised beds including thermal conversion are likely to experience temperatures above 1000 K [149, 150, 151, 152, 153] and therefore, heat transfer through radiation becomes dominant. Toschkoff et al. [154] applied the Discrete Transfer Radiation Model (DTRM) stressed the feasibility of this approach in conjunction with DEM models, however, becomes computationally increasingly expensive with larger numbers of rays [155]. A less expensive and feasible approach was developed by Peters [156, 138] who employed view factors to estimate radiative transfer between a particle and its neighbours. This method was also applied by Fogber and Radl [157] whereby the view factor is estimated based on per-particle corresponding solid angles and treating the particle surface as a black surface. Although a comparison with analytical, Monte-Carlo and OpenFoam solutions agreed well, it is expected that the method still requires a significant CPU time for larger particle arrangements.

A further detailed review on approaches, recent advances and applications is given by Zhong et al. [158]

2. Technological Concept

Numerous challenges in engineering exist and evolve, that include a continuous and discrete phase simultaneously, and therefore, cannot be solved accu-

rately by continuous or discrete approaches, only. Problems that involve both a continuous and a discrete phase are important in applications as diverse as pharmaceutical industry e.g. drug production, agriculture food and processing industry, mining, construction and agricultural machinery, metals manufacturing, energy production and systems biology. Some predominant examples are coffee, corn flakes, nuts, coal, sand, renewable fuels e.g. biomass for energy production and fertilizer. Therefore, the Extended Discrete Element Method (XDEM) provides a platform, that couples discrete and continuous phases for a large number of engineering applications.

The XDEM-suite roots on the Extended Discrete Element Method (XDEM) that is a recently evolved numerical technique. It extends the dynamic properties of the classical discrete element method by additional properties such as thermodynamic state, stress/strain or electro-magnetic field for each discrete entity. Although continuum mechanics approaches are equally applicable, a lack of information is inherent due to averaging of the discrete phase. This loss is usually compensated by additional correlations such as distribution of porosity. However, solutions based on continuum mechanics have the advantage to deal with macro-scale engineering challenges. Methodologies based on DEM-CFD coupling require large computer resources and therefore, deal with applications covering micro- to meso-scales. An analysis of results on smaller scales unveils underlying physics that could be fed into continuum mechanics approaches.

Interaction of the discrete phase with continuous fields via heat, mass and momentum exchange is achieved by a generic interface to the Finite Volume Method (FVM) . A coupling to computational fluid dynamics is based on the software platform of OpenFoam [159] to handle efficiently data transfer between the discrete and continuum phase.

2.1. Fluid Phase Governing Equations

In this regard, the fluid phases are treated as a continuum on macroscopic level using *Eulerian volumetric average* known as multi-fluid model in which the conservation of momentum, mass and energy are solved for each phase separately

[160].The generic governing equation for the k^{th} phase can be written as Eq.(1).

$$\underbrace{\frac{\partial(\epsilon_k \rho_k \phi_k)}{\partial t}}_{transient} + \underbrace{\nabla \cdot (\epsilon_k \rho_k \vec{v_k} \phi_k)}_{convection} = \underbrace{\nabla \cdot \Gamma(\nabla \cdot \epsilon_k \phi_k)}_{diffusion} + \underbrace{S(\phi_k)}_{source/sink} \tag{1}$$

Where the conservation of mass, momentum and energy can be derived by replacing the values in Table 1.

Table 1: Values for conservation equations for each phase

	ϕ	Γ	$S(\phi)$
continuity	1	0	m'
momentum	v	μ	$-\nabla p + F$
energy	h	—	$-\nabla \cdot q + Q$

The term m' is the source term of the continuity equation, represents the mass transfer between phases while the μ and F in the momentum equation are the viscosity and momentum transfer between phases. In the energy equation the diffusivity is described as a term of $q = -\lambda \nabla T$ and λ is the thermal conductivity. The other source term (Q) in the energy equation is any kind of heat transfer between phases. The coupling between the fluid phases and particulate phase is through the *source/sink* term $S(\phi)$ where the positive values represent mass, momentum and energy transfer from the solid particles to the fluid phases and vice versa.

2.2. Governing Equations for the Particle

One-dimensional and transient conservation equations characterize energy and mass transport within each particle. Conservation of mass for gas within the pore volume of a porous particle writes as follows:

$$\frac{\partial}{\partial t}\big(\varepsilon_p \rho_g\big) + \tag{2}$$

where S_{mass} is the summation of the individual species mass production or consumption rates created by chemical reactions. ε_p denotes particle porosity and u_g advective velocity. Moreover, the fluid's intrinsic density ρ_g is given by

the sum of partial densities of species present in the gas phase as $\rho_g = \sum_i \rho_{i,g}$. Transport of gaseous species within the pore space of the particle is considered to obey Darcys law:

$$-\frac{\partial p}{\partial r} = \frac{\mu_g \epsilon_p}{K} \langle u_g \rangle \tag{3}$$

where p is pressure and μ_g denotes the dynamic viscosity and K represents the permeability of the porous particle. The balance of an individual specie i within the pores of a given particle is described by

$$\frac{\partial(\epsilon_p \rho_{i,g})}{\partial t} + \frac{1}{r^n}\frac{\partial}{\partial r}(r^n \epsilon_p \rho_{i,g} u_g) = \frac{1}{r^n}\frac{\partial}{\partial r}(r^n D_i \epsilon_p \frac{\partial}{\partial r}\rho_{i,g}) + \epsilon_p \sum_k \dot{\omega}_{k,i,g} \tag{4}$$

where $\dot{\omega}_{k,i}$ denotes the source term accounting for the consumption or generation of species i from reaction k and D_i is the molecular diffusion coefficient. The distribution of temperature within a single particle is accounted for by the energy equation as:

$$\frac{\partial}{\partial t}(\rho h) = \frac{1}{r^n}\frac{\partial}{\partial r}\left(r^n \lambda_{\text{eff}} \frac{\partial T}{\partial r}\right) + Q' \tag{5}$$

$$Q' = \begin{cases} \sum_{k=1}^{l} \dot{\omega}_k H_k & \text{in case of chemical reaction} \\ -m' h_{l,m} - m' L_f & \text{in case of melting} \end{cases} \tag{6}$$

where λ_{eff} is the effective thermal conductivity and $h_{l,m}$, L_f and H_k donate the enthalpy of the liquid at melting temperature, latent heat of fusion, and the enthalpy of reaction, respectively. m' is the melting rate which will be defined later. To solve the equations, the following boundary conditions are needed:

$$-\lambda_{\text{eff}} \frac{\partial T}{\partial r}\bigg|_{r=0} = 0 \tag{7}$$

$$-D_i \frac{\partial \rho_{i,g}}{\partial r}\bigg|_{r=0} = 0 \tag{8}$$

$$-\lambda_{\text{eff}} \frac{\partial T}{\partial r}\bigg|_{r=R} = \alpha(T_s - T_\infty) + \dot{q}''_{\text{rad}} + \dot{q}''_{\text{cond}} \tag{9}$$

$$-D_i \frac{\partial \rho_{i,g}}{\partial r}\bigg|_{r=R} = \beta_i(\rho_{i,s} - \rho_{i,\infty}) + \dot{m}''_{i,g} \tag{10}$$

where α and β denote the heat and mass transfer coefficients, T_∞, $\rho_{i,\infty}$ represent the ambient gas temperature and the gas partial density of the species i in ambient gas. T_s, $\rho_{i,s}$ donate the particle temperature and the partial density of species i at the surface of the particle, respectively. $\dot{m}''_{i,g}$ accounts for the mass fluxes from the environment. Moreover, $\dot{q}''_{\text{rad}}$ and $\dot{q}''_{\text{cond}}$ account for conductive heat and radiation transport through physical contact with the wall and/or particles and are calculated as follow:

$$\dot{q}''_{p,\text{rad}} = \sum_{j=1}^{M} F_{p\to j}\sigma\left(T_p^4 - T_j^4\right) \tag{11}$$

$$\dot{q}''_{p,\text{cond}} = \sum_{j=1}^{N} \frac{1}{\frac{1}{\lambda_p} + \frac{1}{\lambda_j}} \frac{T_p - T_j}{\Delta x_{p,j}} \tag{12}$$

where $F_{p\to j}$ is the view factor between particle p and its neighbor j and λ is the thermal conductivities of the different particles. The equations are conveniently written to be represented on different coordinates systems. Thus, the particle geometry can be chosen to be an infinite plate $n = 0$, infinite cylinder $n = 1$ or a sphere $n = 2$.

The discrete element method based on the soft sphere model is applied to the dynamic module of the XDEM-suite. The movement of each particle is tracked using the equations of classical mechanics. Newtons and Euler's second law for translation and rotation of each particle are integrated over time and the particle positions, orientations and velocity are updated accordingly during time integration.

$$m_i \frac{d\vec{v_i}}{dt} = m_i \frac{d^2\vec{x_i}}{dt^2} = \vec{F}_i^c + \vec{F}_i^g + \vec{F}_i^{ext} \tag{13}$$

$$I_i \frac{d\omega_i}{dt} = \sum_{j=1}^{n} M_{i,j} \tag{14}$$

where $\vec{F}_i^c$, $M_{i.j}$, $\vec{F}_i^{ext}$, v_i, ω_i, I_i are contact forces, torques and external forces acting on particle i, linear velocity, angular velocity and moment of inertia, respectively. For more description the reader is referred to [161, 162, 163, 164]

Transport coefficients, thermodynamic and other properties are spatially resolved to include dependencies such as temperature and are available from an extensive data base including NASA polynomials for solid, liquid and gaseous species.

3. Engineering Applications

The following section addresses relevant and validated applications that emphasise the predictive capabilities of the XDEM-suite.

3.1. Generic Multi-phase Flow Solver

The multi-phase solver of the XDEM-suite is applicable to any system including several fluid phases flowing through packed bed of solid particles, which exist in broad spectrum of engineering disciplines as was mentioned before. The frequently used reactors of these types are packed bed, trickle bed, fluidized bed reactors which can be classified as counter-current, co-current and cross-current based on the direction of the fluid phases [165].

The flow behaviour in packed bed reactors is very complex and depends not only on hydrodynamics but also on the mass and heat transfer between all phases [166]. The size parameter and geometry of the particulate phase have a pronounced effect on the flow distribution of fluid phases [167, 166, 168]. In order to predict the performance of these reactors, the local interaction between all phases such as fluid-fluid, fluid-solid and solid-solid interactions must be taken into account. The Eulerian-Lagrangian characteristics of the XDEM-suite allow including all these interactions for any particulate system.

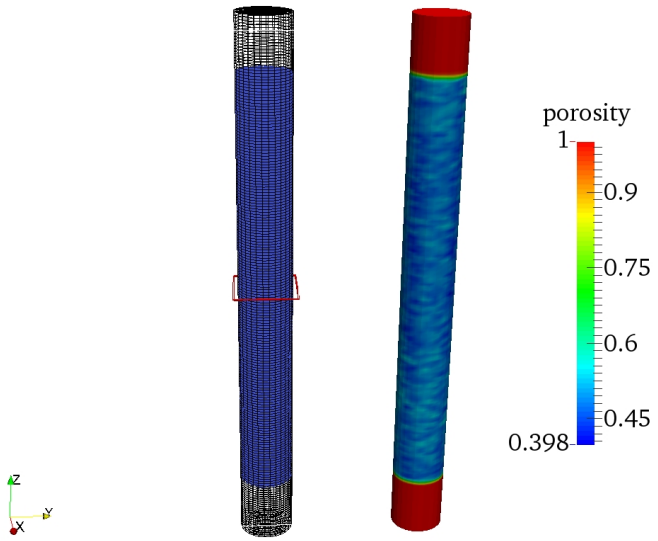

Figure 1: Computational domain and porosity distribution

The generic solver was validated using experimental data of Gunjal et al. [169] for flow of air and water at room temperature through packed bed of solid particles. An experiment was carried out in a vertical pipe filled with $6mm$ spherical particles to represent trickle bed reactors. The geometry of the case as well as the position of the particles are shown in fig. 1 that includes also the distribution of porosity . The XDEM-suite calculate the porosity of each CFD cell based on the algorithm proposed by Xiao et al. [170].

The results were validated by comparing predicted results versus experimental data for pressure drop and liquid hold up. In fig. 2, the pressure drop for different liquid velocities is shown, which confirms that by increasing the liquid velocities, the pressure drop increases as well. In fig. 3, the liquid hold up against liquid velocity is depicted, which shows that higher liquid hold up occurs when higher liquid velocity is introduced. Both figures show a very good agreement with experimental data.

In order to visualize other hydrodynamic parameters such as velocities and saturations, a slice at height of 0.5 m (shown in fig. 1) for a specific case was

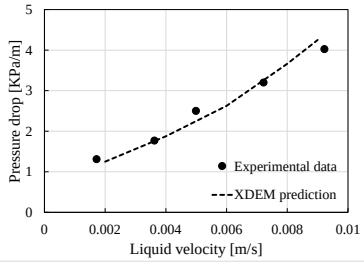

Figure 2: The XDEM prediction for pressure drop vs experimental data of Gunjal et al. [169]

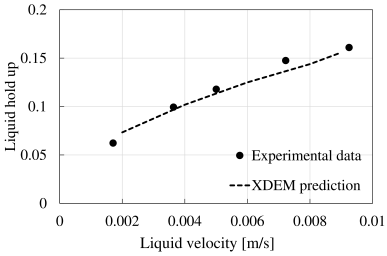

Figure 3: The XDEM prediction for liquid saturation vs experimental data of Gunjal et al. [169]

chosen, which are displayed in fig. 4. The porosity distribution for this slice is depicted in fig. 4(a) and it is drawn over a line in fig. 4(b) in order to show the wall effects. As it is clear in part (b), higher porosities are observed at the vicinity of the wall, which highly effect the hydrodynamic parameters as compared to a constant porosity distribution. The liquid and gas phase velocities are shown in part (c) and (d) respectively, while phase saturations are depicted in part (e) and (f). Higher velocities are in respect to higher saturation zones. The non-uniform velocity profiles represent the effect of equally non-uniform porosity distribution estimated by the XDEM-suite which leads to more accurate and precise prediction of hydrodynamic parameters. More details about the multiphase solver of the XDEM suit can be found in [171, 172, 173].

3.2. Melting of particles as Phase Change Including Heat and Mass Transfer

Transport phenomena including a phase change such as evaporation, melting and solidification play a key role in a wide range of engineering applications among which melting is of particular interest and addressed in this section.

A melting process is found in many industrial processes such as metal processing, environmental engineering and thermal energy storage systems where three phases of solid, liquid and gas could exist simultaneously. These systems are difficult to model with numerical analysis due to the complex interaction between the different fluid phases and the granular phase. As was discussed be-

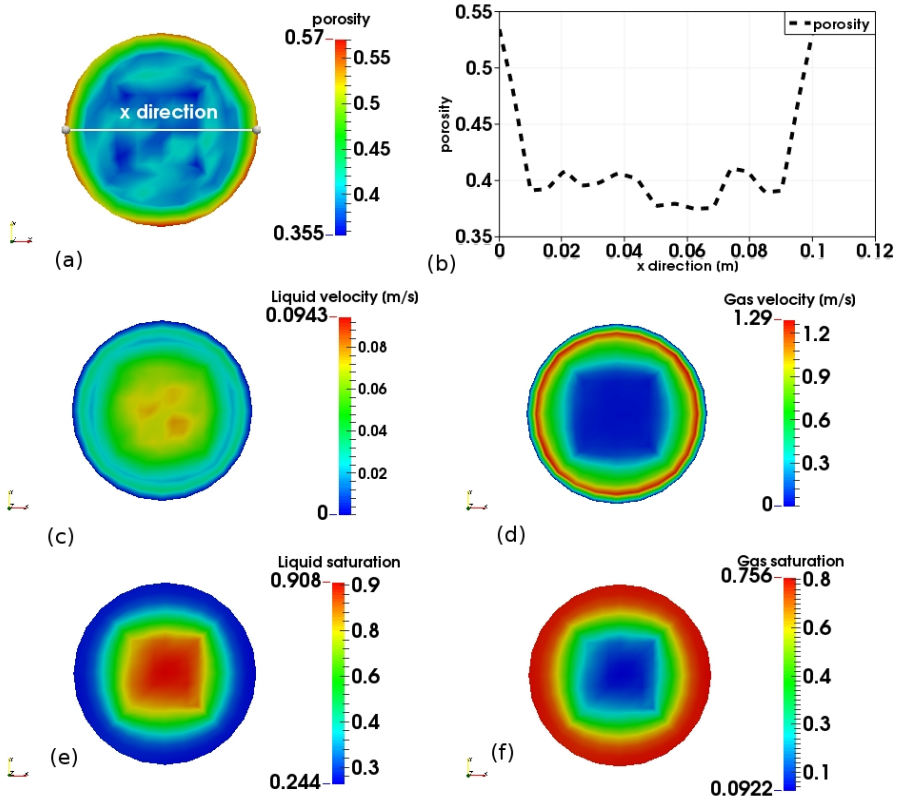

Figure 4: (a) porosity distribusion, (b) porosity distribusion over a line depicted in part (a), (c) liquid phase velocity, (d) gas phase velocity, (e) liquid phase saturation, (f) gas phase saturation

fore, the Lagrangian-Eulerian framework is closer to the real physical processes rather than the Eulerian-Eulerian model for granular flows which includes particle - particle interaction. These kind of process can be modelled using the XDEM-suite, Since the XDEM-suite is an Eulerian-Lagrangian platform which includes heat, mass and momentum transfer between the fluid phases and solid particles.

where h_{sl}, m' and h_{lm} are latent heat of melting, the melting rate and specific enthalpy of melt, respectively. The melting rate m' in the energy equation can be estimated based on a the energy balance. It requires that the latent heat of melting is related to heat transfer to particle. Heat available above the melting temperature is consumed by melting process [173, 174]. Therefore, a melting rate is defined as:

$$m' = \begin{cases} \frac{\rho(h-h_m)}{L_f \Delta t} & h \geq h_m \\ 0 & h < h_m \end{cases} \tag{15}$$

where h and h_m are the enthalpy of particle at the particle's temperature and melting temperature, respectively. The melting rate m' and $m'h_{lm}$ are transferred to the CFD field by introducing a source term in the liquid continuity and energy equations for the fluid phases the governing equations of the multiphase solver discussed in the previous section.

The new radius of the particle is estimated based on the mass loss at the surface in each time step. It is assumed that the particle retains its sphericity in the whole process.

Validation was performed employing experimental study conducted by Shukla et al. [175]. The case was considered according to the experimental study under the influence of forced convection for which the set up is shown in fig. 5. The experiment was carried on a single sphere ice particle with an initial diameter of 0.036 m fixed in a open channel with dimensions of 500, 152, 216 mm. Water with a velocity of 0.06 m/s passed the ice sphere horizontally and temperature of the surrounding water, the melting temperature and initial temperature of

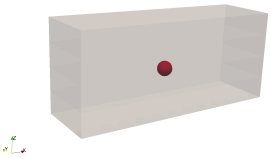

Figure 5: Experimental setup for a single particle in a free stream of water.

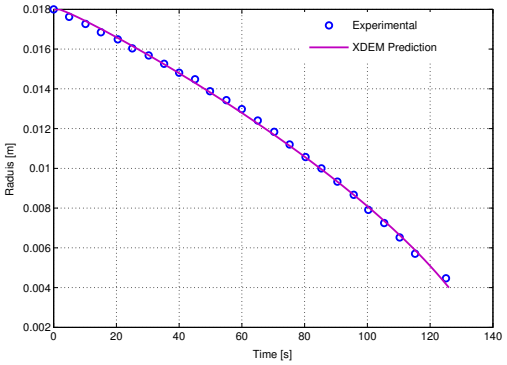

Figure 6: Time history of the radius of the single ice particle.

the ice particle were set to 299.15 K, 273.15 K and 257.15 K, respectively. Latent heat of melting of ice is considered to be 334 $\frac{KJ}{Kg}$.

Fig. 6 depicts the comparison between experimental data and the predicted results for the ice spheres radius versus time which shows excellent agreement. A time step of 0.005 second was used in calculations. Lower values of a time step produced similar result. In addition, the model has been applied for melting of a packed bed of ice particles. The water with the velocity of 0.01 m/s and the temperature of 320.15 K enters from the top of a box with dimensions of 300 mm in width, 152 mm in depth and 100 mm in height, and flows through an assemble of particles. The water temperature distribution and the size of particles are presented in fig. 7 for different instances.

The results include temperature distributions in both fluid and individual particles, that additionally experience forces due to collisions and buoyancy. Thus, the model framework within the XDEM-suite takes into account all relevant physics and predicts accurate results.

3.3. Powder Metallurgy

Mining, forming and cutting tools as well as wear resistant tools are some of the most important products of the hard metal industry. One of the most employed materials in the hard metal industry is tungsten carbide (WC). Tungsten carbide is a hard composite that ensures resistance to wear, deformation

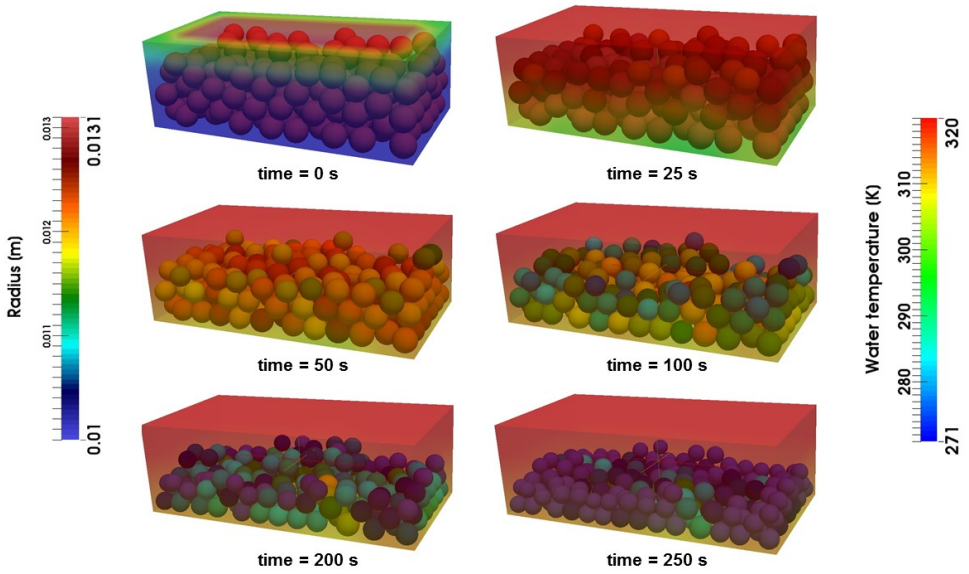

Figure 7: Particles size and temperature at different times.

and fracture to the demanding applications. During sintering of WC small grains may dissolve and larger grains grow resulting in an overall increase of the grain size. According to the sintering conditions, the grains tend to grow differently and some individual grains may even grow to an uncommonly large size compared to the average grain size. Abnormal large grains negatively impact most the mechanical properties of tungsten carbides, because they may act as initiation points for breakage. The WC grain size distribution is essentially determined by the grain size distribution of the employed tungsten powder [176]. Thus, one of the major challenges in carbide technology is to control the grain size of tungsten powder effectively and accurately.

Tungsten powders are industrially produced by reduction of tungsten oxides, almost exclusively, via hydrogen reduction of tungsten blue oxide (TBO)[177]. The tungsten blue oxide is not a standard defined tungsten oxide with a chemical composition that depends on the production conditions from its precursor APT [176]. The size of the reduced tungsten powder is governed by the prescribed humidity, temperature of the process, height and morphology of the tungsten

oxides powder beds, the flow of the feedstock, the direction and flow of the reducing agents and the dew point [176, 177, 178]. The reducing hydrogen-flow does not only drive the reduction process, but it also removes the formed water vapour. The retention of water vapour within the powder is one of the most important factors to control because water vapour can react with the existing oxides forming the volatile compound $WO_2(OH)_2$, which is transported and deposited in different localities [176]; influencing directly the widening of the tungsten grain size distribution including abnormally large grains. Thus, controlling the water vapour production and retention during the reduction process is of pivotal interest and immediate industrial impact. In order to study this process, scientists have developed models to gain understanding and to try to control the phenomena. Nowadays, literature offers empirical models that rely on theoretical diffusion equations described in terms of temperature, time, diffusion-path lengths, and oxide bulk density to predict the extent of heterogeneous reactions. However, due to the lack of a comprehensive and accurate representation, industrial production today is still relies on empirical knowledge [179].

In this section the XDEM-suite is employed to describe the tungsten powder production under industrial like conditions. Hydrogen reduction of WO_3 to W-powder is considered a well-established process [176, 180, 181]. The chemical conversion of WO_3 powder is represented by a staged-mechanism, reactions (8) to (11) [182], where oxygen is removed out of the system in the form of water vapour.

$$WO_3(s) + 0.1H_2(g) \rightleftarrows WO_{2.9}(s) + 0.1H_2O \tag{16}$$

$$WO_{2.9}(s) + 0.18H_2(g) \rightleftarrows WO_{2.72}(s) + 0.18H_2O \tag{17}$$

$$WO_{2.72}(s) + 0.72H_2(g) \rightleftarrows WO_2(s) + 0.72H_2O \tag{18}$$

$$WO_2(s) + 2H_2(g) \rightleftarrows W(s) + 2H_2O \tag{19}$$

Each of the above-inserted reversible bi-molecular reactions can be treated as equilibrium bi-molecular and finite rate reactions. For such a reaction model the reaction rate, or the concentration rate of a species k, involved in an equilibrium reaction at temperature T is represented by the following differential relation

$$\frac{dc_k}{dt} = k_f(T) \cdot \left(\nu'_k \cdot \prod_{i=1}^{N} c_{R_i}^{\nu'_i} - \frac{\nu''_k}{K_{\mathrm{eq,c}}(T)} \cdot \prod_{j=1}^{M} c_{P_j}^{\nu''_j} \right) \tag{20}$$

where N denotes the number of reactants R_i, M denotes the number of products P_j, $\nu_{i/j}$ represents the absolute values of the corresponding stoichiometric coefficients and $k_f(T)$ denotes the Arrhenius coefficient [183].

The WO_2 powder employed for this study was prepared prior to experimentation. The selected tungsten oxide reduction step is the dominant part occurring during the industrial production of tungsten powders. Table 2 summarizes the experimental as well as the numerical setup of the above-mentioned experiments.

Table 2: Numerical properties selected during WO_2 reduction simulation

Powder		
WO_2	98	%
Size	35	μm
Total mass	100	g
Reducing gas		
H_2	99.9	%
Volumetric flow	15	Nm^3/s
Powder bed		
Height	10	mm

In order to show the predictive capabilities of the method, XDEM predictions are compared to measurements of water vapour. Fig. 8 successfully validates the presented approach for the industrial reduction of tungsten oxides. In the figure, the experimental data of the water vapour mass fraction was taken from continuous humidity measurements in the outlet gases. The filtered data, was obtained after passing the signal measurement through a simple moving-average

filtering algorithm. In this case study, water vapour is a product of the hydrogen reduction of WO_2. Hydrogen is applied in excess to drive the reaction progress and evacuate the produced water vapour. Consequently, and as described in eq. 19, the concentration of water vapour indicates the oxygen removal, and therefore, the reaction progress. Due to the high gas flow, industry assumes that outlet measurements are highly representative of the water concentration inside the furnace, and consequently, indicates the reactions progress. The high correlation between measurements and predictions not only validates the numerical predictions, but also indicates that outlet measurements are consistent with the intra-furnace reduction process.

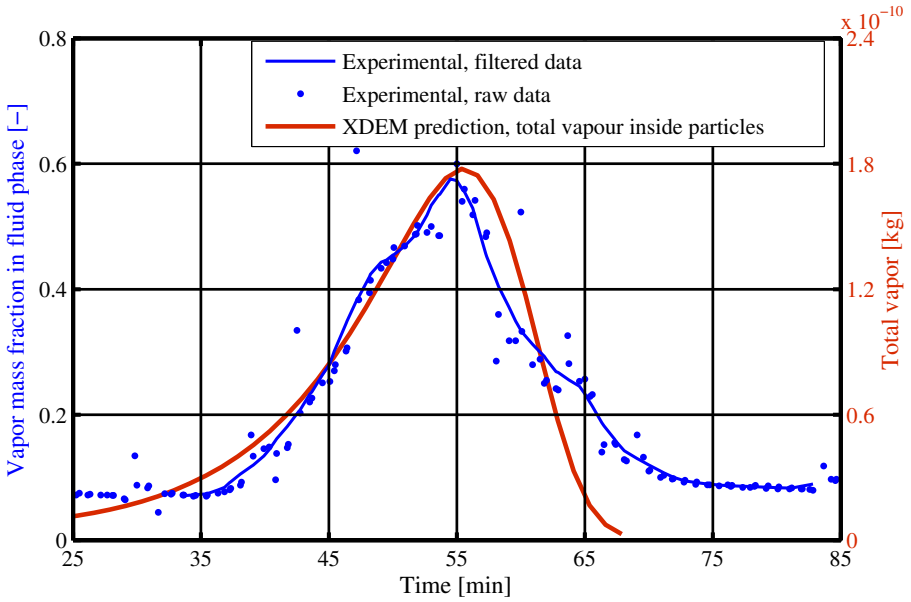

Figure 8: Comparison of water vapour predicted by XDEM-suite and experimental measurements in gas outlet. The prediction for total water vapour in the powder bed is plotted in red and blue lines describe water vapour mass fraction measured at the outlet of the furnace.

These results as well as previous validations documented in [179, 182, 184] anticipate that employing the XDEM methodology combined with experimental data provides important breakthroughs for the powder metallurgy industry.

3.4. Thermal Treatment of Biomass

Thermal treatment of biomass refers to the conversion of biomass when the essential heat is available in the system. In this case, physical and chemical processes shown in fig. 9 as heat-up, drying, pyrolysis, combustion and gasification take place.

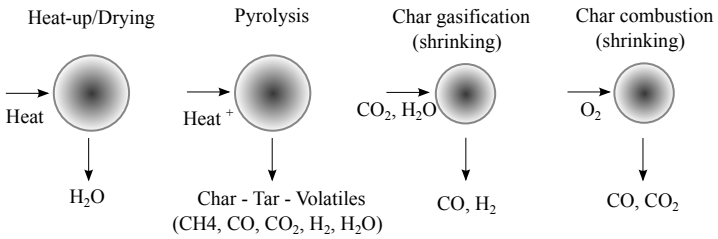

Figure 9: Main steps of conversion process

Heat-up is warming biomass to increase the temperature above the ambient temperature. When the surface temperature of biomass reaches the saturation status (around 100° C at 1 bar), the water contents of biomass start to vaporize whereby the drying process begins. After removing the water content and with increasing heat, the biomass starts to decompose thermally to solid char, liquid tar and volatile gases ($CH_4, CO, CO_2, H_2, H_2O$). This stage is pyrolysis or devolatilization process. The released heat from reactions between the volatile gases and oxygen is used for drying and pyrolysis of new feeding biomass fuel to the reactor and producing further volatiles so that this cycle continues as far as the oxygen is provided to the system. The remaining char from thermal decomposition is gasified via reacting with CO_2 and H_2O to generate useful gases of CO and H_2 which are highly combustible. Also char is oxidized at high temperature above 700° C denoting the combustion process when the solid char reacts with oxygen. [185]

Here the XDEM-suite is applied to validate the drying of a single particle with the experiment carried out by Looi et al. [186]. The particle is considered as a spherical wet particle including 60 % of moisture content and diameters $10, 12$ mm defined as cases **A** and **B**. The experiments are performed at the

pressure of 2.4 bar, and the superheated steam temperature at 170° C, as well as the steam velocity at 2.7 m/s.

The prediction of particle core temperature compared to experiment is shown in fig. 10 that shows a very good agreement.

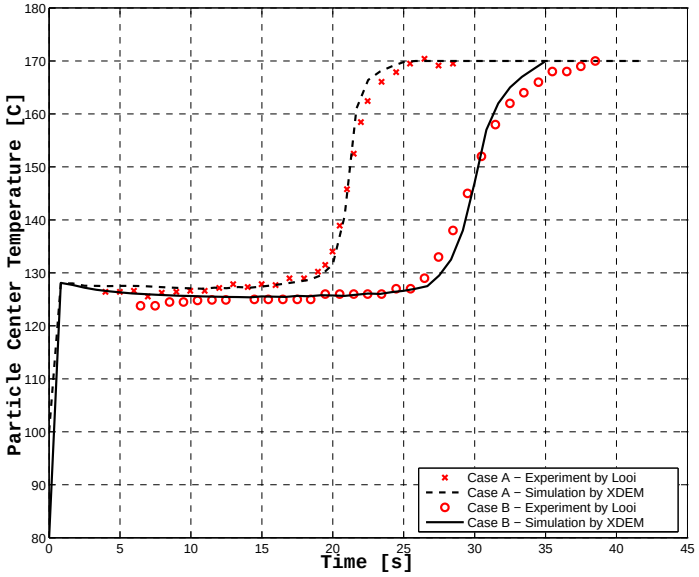

Figure 10: Particle size effect on drying of a coal particle— Case A: $d_p = 10mm$, $P = 2.4bar$, $T_a = 170°C$, $v_g = 2.7m/s$; Case B: $d_p = 12mm$, $P = 2.4bar$, $T_a = 170°C$, $v_g = 2.7m/s$

In case **A**, the temperature rises from saturation after 20 s while in case **B** it rises after 27 s which states that the small particle is dried faster. The reason is in the small particle, heat transfer from the surface to core of particle is faster. However, the temperature of particles in both cases reaches the gas temperature (170° C) at the end of drying. In addition, fig. 11 shows the behaviour of drying rate based on the moisture content for case **B**. The AB part on the curve represents a warming-up period of the particle. The BC part is the constant-rate period where the particle temperature is constant during this period since heat transfer into the surface is constant and the heat is consumed just for water evaporation. When the free water is finished, the temperature starts to rise. This point is shown as point C, where the constant-rate ends and the drying rate begins falling that is termed the critical-moisture content.

The curved portion CD is termed the falling-rate period and is typified by a continuously changing rate throughout the remainder of the drying cycle. In addition, fig. 11 depicts the predicted residual moisture content which agrees w

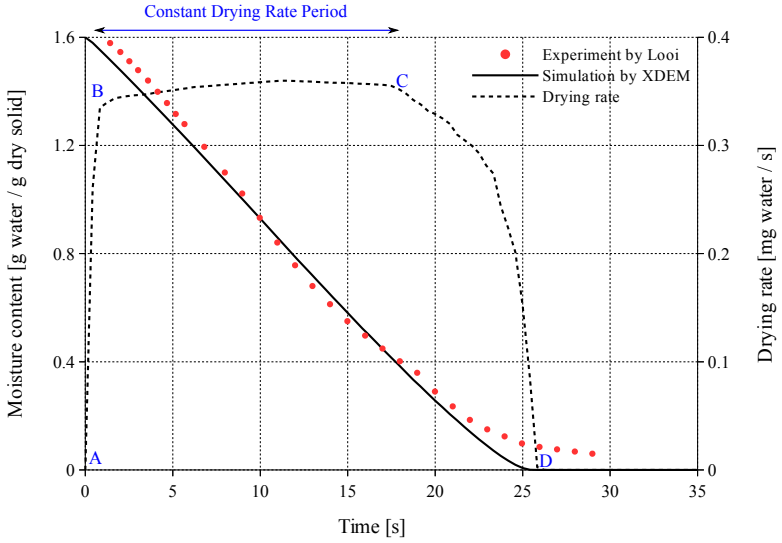

Figure 11: Drying rate and moisture content vs. time— case **B**: $d_p = 12mm$, $P = 2.4bar$, $T_a = 170°C$, $v_g = 2.7m/s$

3.5. Dual-grid multiscale simulations of three-phase flows

The dual-grid multiscale approach for three phase flows was introduced in [188, 189] and applied to several flow configurations ranging from conventional process engineering [190] to additive manufacturing [191]. It consists in the identification of two length-scales: a bulk scale where the coupling between CFD and DEM domain is preformed, and a fluid fine scale at which the fluid equations are resolved. One CFD grid is associated to each scale, making the grid used for the solution of the fluid flow equations independent from the particles' characteristic dimension. In [188] was shown how, by adopting a correct interpolation strategy between the two grids, the multiscale approach can produce accurate, grid-convergent results when the standard DEM-VOF method cannot.

3.5.1. Laminar three-phase dam-break

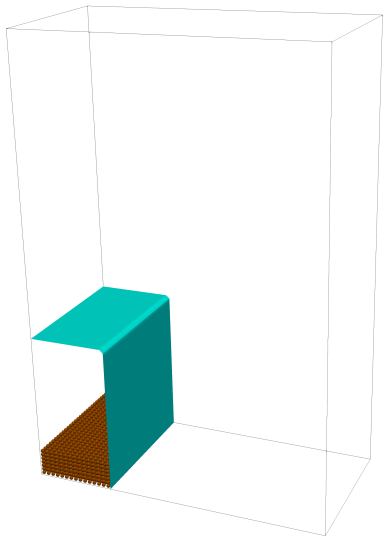

Figure 12: Dual-grid multiscale simulation of three-phase flows: Laminar dam-break setup as in [188] .

The dam break is a famous benchmark for multiphase flows, that was proposed in various configurations by different authors [192]. In particular its

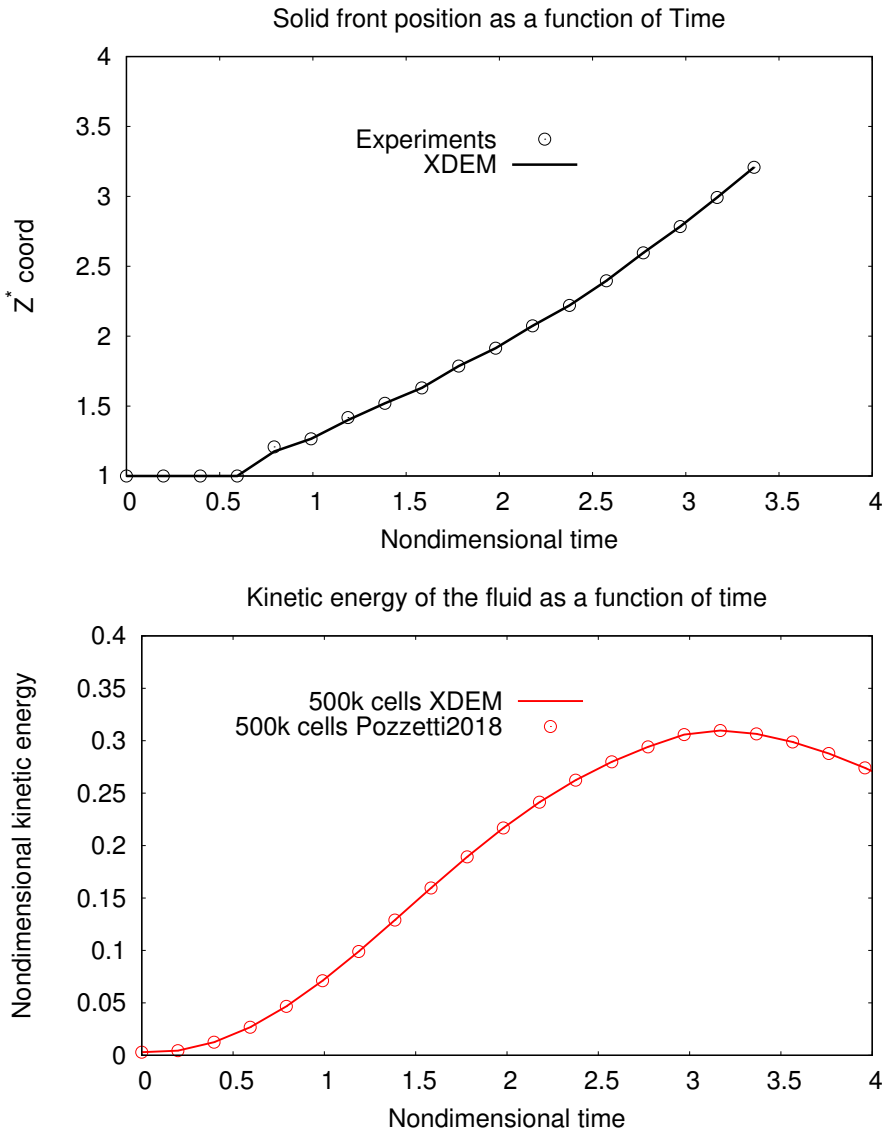

Figure 13: Dual-grid multiscale simulation of three-phase flows: Comparison between the reference results in [188] and the implementation within the XDEM platform.

extension to three-phase flows has been of great interest for civil/chemical engineering. We here re-propose a dam-break benchmark as introduced in [188] and citations within, resolved with the dual-grid multiscale DEM-VOF solver

of the XDEM-platform. The benchmark features a box of dimensions $0.2m$ x $0.1m$ x $0.3m$, where column of water of $0.05m$ x $0.1m$ x $0.1m$, and an uniformly distributed bed of spherical particles at the bottom, breaks and stabilizes. The spheres have a diameter of $2.7\,mm$. As already done in [188] we refer to and adimensional kinetic energy:

$$\mathbf{E_{kin}} = \frac{\int_D \mathbf{u}_f \cdot \mathbf{u}_f \, \rho_f \frac{1}{2} dV}{\int_{Z_{col}} A_{in} \rho_h g dZ}. \tag{21}$$

The nondimensional time is defined as

$$t^* = t \left(\frac{2g}{a} \right)^{\frac{1}{2}}, \tag{22}$$

with $a = 0.05m$. In figure 13, one can observe how the benchmark is satisfied by the XDEM-platform in terms of accuracy in the prediction of the experiments, and of convergence to the reference value of the kinetic energy.

3.5.2. LES approach to turbulent flows

Industrially-significant flows often have to deal with high velocities. This represents a major problem for the numerical approach to such flows as the non-linearity of the Navier-Stokes equations can trigger physical and numerical instabilities [193]. Different numerical approaches have been proposed to cope with this problems, for a detailed description of which the reader is referred to [193] and citations within. For a numerical treatment of turbulent phenomena within multiphase flow, the Large Eddy Simulation (LES) approach have been found to hold interesting advantages [194]. The LES approach aims to compute exactly the large, energy-carrying structures of the flow, while modeling the smaller scales whose behaviour is accepted to be less local [193]. This is obtained by a filtering operation applied on every field variable

$$\tilde{\mathbf{y}}(\mathbf{x}) = \int_A \mathbf{y}(\mathbf{x}') \Phi(\mathbf{x}, \mathbf{x}', \tilde{\Delta}) d\mathbf{x}', \tag{23}$$

where A is the domain of the simulation, Φ a generic filter, with $\tilde{\Delta}$ the filter width. This allows to ideally divide the velocity vector field as

$$\mathbf{u}_f(\mathbf{x}) = \tilde{\mathbf{u}_f}(\mathbf{x}) + \mathbf{u}'_f(\mathbf{x}), \tag{24}$$

with $\tilde{\mathbf{u}_f}(\mathbf{x})$ the filtered term as in 23, and $\mathbf{u}'_f(\mathbf{x})$ the remaining contribute whose effects need to be modelled.

Classical turbulence models effectively succeeded in describing the effects of unresolved structures on the resolved ones. If a dispersed phase is present in the flow the effect of the unresolved structures on the particle may be addressed by reconstructing a stochastic unresolved velocity field using information about the turbulent kinetic energy [195, 196, 197, 198]. The XDEM platform allows to perform coupling between a discrete phase and a LES solution both considering only the resolved structures as relevant for the flow, and therefore using the filtered velocity as coupling variable, or taking into account an average effect of the unresolved scales by partially reconstructing a sub-grid velocity field.

The partially reconstructed velocity field can be used in order to calculate the drag force in the form

$$\tilde{\mathbf{u}'_f} = \quad \tilde{\mathbf{u}'_f}(\mathbf{k}), \tag{25}$$

$$\tilde{\mathbf{u}_f} = \quad < \mathbf{u}_f > + \tilde{\mathbf{u}'_f}, \tag{26}$$

$$F_{drag} = \quad F_{drag}(\tilde{\mathbf{u}_f}), \tag{27}$$

with $\mathbf{k}$ the turbulent kinetic energy One of the simplest reconstruction procedure can be obtained by

$$\tilde{\mathbf{u}_f}'_i = \quad \sqrt{\tfrac{2}{3}\mathbf{k}}\,\psi_i \; for \; i = 1, .., 3, \tag{28}$$

with ψ_i being a white noise. This assumes the subgrid-scales to be perfectly isotropic and the different components of $\tilde{\mathbf{u}_f}$ to be uncorrelated.

The standard two-phase dam break usually involves an obstacle against

which the water column is breaking. We propose a similar benchmark test by substituting the obstacle with a pile of particles. The water column is breaking against the pile of particles, lifting them, and transporting them in a slurry flow that impacts on the wall. The setup for the simulations include a domain size of $10\,m$ x $2\,m$ x $3\,m$ initially the water is at $5\,m$ x $2\,m$ x $2\,m$. A block of 700 particles of $10\,cm$ diameter, consisting in seven layers of 10 x 10 reticulates is posed at $1\,m$ of distance from the dam. The particles density is fixed at $800\,kg/m^3$. Considering the actual dimensions of the domain the problem could not be solved with laminar assumptions. The LES scheme described in the previous section is used. We propose results for a sub-domain discretisation of $150k$ and $500k$ hexahedral piecewise constant elements. In figure 14 the evolution of the dam break is shown.

Three configurations are compared: the dam in absence of particles, and at the presence of particles with different domain discretisation. It can be noticed how the flow configuration changes completely at the presence of the particle, in particular the water partially filters through the bed while lifting the particles. One can observe how the discretisation of the domain changes not only the resolution of the liquid-gas interface, but as well the velocity distribution of the particles. In fig. 15 the interface area as a function of time is shown for the three cases.

It can be noticed how the presence of the particle obstacle significantly changes the qualitative behaviour of the dam breaking, causing a premature rupture of the interface (approximatively around $t = 0.5s$) with consequent increment of the interface area. At the same time the usage of a finer discretisation allows to capture smaller structures and therefore leads to an higher interface area prediction. In figure 16 and 17 the profiles for the total kinetic energy and the sub-filter kinetic energy of the system are presented.

It can be noticed how the total kinetic energy of the fluid system is influenced by the particle presence. In particular areas where the particles are storing kinetic energy from the fluid (and the profiles are are under the curve relative to the water at $t = 0.5 - 0.9$ and $t = 1.2 - 2.7$) and areas where the particles are

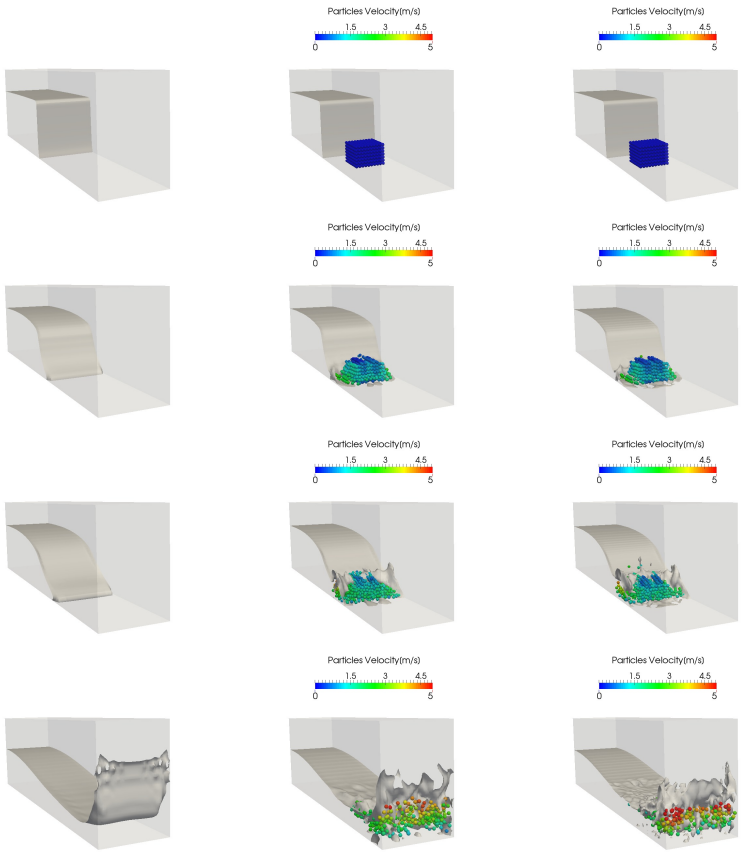

Figure 14: Dam breaking against a pile of particles significant time step. Comparison between a Dam without obstacles (left), and with obstacle and subdomain discretization of $150k$ elements (middle) and $500k$ elements(right). From the top to the bottom are shown times of $0.1s$, $0.35s$, $0.50s$, $0.85s$.

releasing kinetic energy into the fluid (approximatively for times $t = 1.1 - 1.3s$ and $t = 3 - 4s$) can be observed. With reference to fig. 16 the turbulent kinetic energy appears correctly bounded. Looking at fig. 17 one can notice how the presence of the particle influences the turbulence kinetic energy profile. Comparing the behaviour of the system with only water and the one with particles and a discretisation of 150000 element (that is also the one adopted for the dam without particles), a qualitatively different time distribution of the subfilter kinetic energy is observed. In particular during the impact with the wall at $\mathbf{x} = 10m$ a higher subgrid kinetic energy can be observed when particles

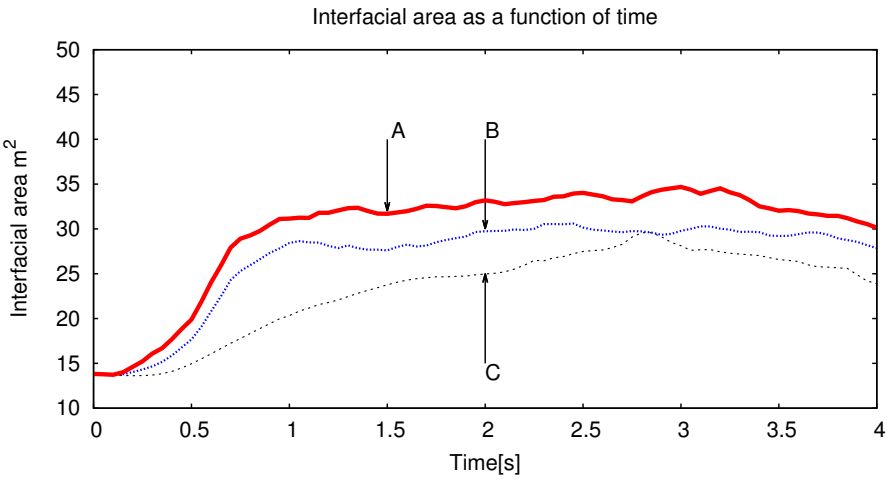

Figure 15: Turbulent Dam Break: Interface area as a function of time, Comparison between a sub-domain discretisation of $500k$ elements (A), $150k$ elements(B), and a dam without obstacle (C).

are present in the system. In reverse during the second impact with the wall at $\mathbf{x} = 0$ the sub-filter kinetic energy is higher for the pure fluid, while the presence of the particles gives now to the fluid a more viscous behaviour. By comparison between the two different discretisation of the fluid-particle system, one can notice how the contribution of the sub-filter kinetic energy decrease when a finer discretisation is adopted, while the qualitative behaviour remains similar. This is in accordance to the general LES theory since a finer discretisation allows to resolve more scales, and therefore a bigger part of the total kinetic energy.

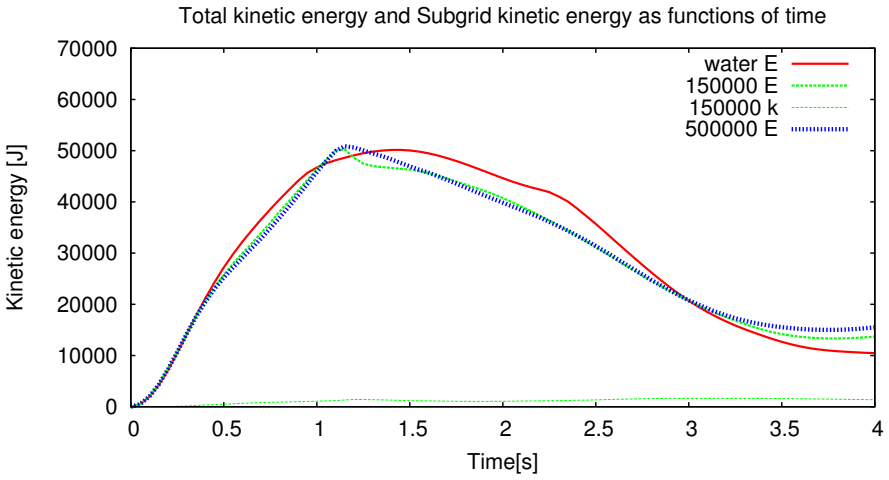

Figure 16: Turbulent Dam Break. Total kinetic energy (E) as a function of time, Comparison between a subdomain discretization of $500k$ elements (500000), $150k$ elements(1500.000), and a dam without obstacle (water). The sub-filter kinetic energy (k) for the discretization of $150k$ elements is shown as a comparison term.

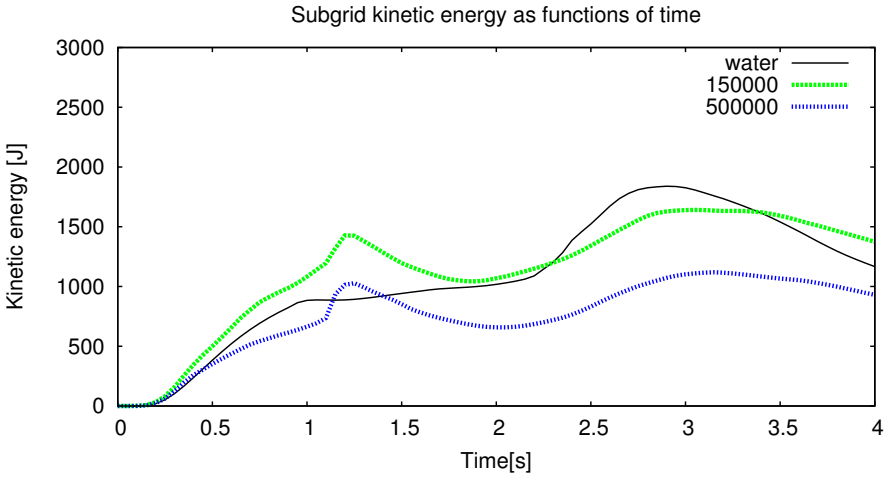

Figure 17: Turbulent Dam Break. Total sub-filter kinetic energy (k) as a function of time, Comparison between a subdomain discretization of $500k$ elements (500000), $150k$ elements(150000), and a dam without obstacle (water).

4. Summary

This contribution reviews relevant literature addressing multi-phase flow with a solid phase as particulate material present. In addition, the article introduces the predictive capabilities of the XDEM-suite applied to a solid phase that is closely linked to the fluid phase by an intensive heat, mass and momentum transfer. The interface between continuum and discrete numerical approaches includes a selection of fluid dynamic solvers and a variety of different and fundamental reaction mechanism that cover a large number of numerical approaches to describe thermal conversion of a particulate phase. Approaches presented are validated with experimental data, that establishes an accurate framework for investigating a variety of engineering applications. Results obtained exhibit a large degree of detail, in particular on smallest scales. A thorough analysis of the results obtained allows unveiling the underlying physics, that enables engineers to improve both design and performance.

5. Acknowledgements

The authors would like to acknowledge the support of Fond National de la Recherche Luxembourg, Europe FP7 IAPP program (Grant IAP-GA-2012-323526-AMST) and the HPC centre of the University of Luxembourg.

References

References

[1] R. D. Blevins, Applied Fluid Dynamics Handbook, Krieger Publishing Company, Malabar, Florida, 1984.

[2] J. H. Ferzinger, M. Peric, Computation Methods for Fluid Dynamics, Springer Verlag, Heidelberg, 1996.

[3] K. J. Bathe, Finite Element Procedures, Prentice Hall, 1996.

[4] O. Zienkiewicz, Methode der Finiten Elemente, Carl Hanser Verlag, 1984.

[5] D. Gidaspow, Multiphase flow and Fluidisation, Academic Press, 1994.

[6] B. Peters, Thermal Conversion of Solid Fuels, WIT Press, Southampton, 2003.

[7] Power Generation from Solid Fuels, Springer-Verlag Berlin Heidelberg, 2010.

[8] Y. Omori, Blast Furnace Phenomena and Modelling, Elsevier, London, UK, 1987.

[9] J. Szekely, Y. Kajiwara, A mathematical representation of spatially non-uniform, counter-current flow of gases and liquids in packed beds-of relevance to flow phenomena in the bosh of iron blast furnaces, Trans Iron Steel Inst. 19.

[10] T. Sugiyama, M. Sugata, Development of two-dimensional mathematical model for the blast-furnace, Tech. Rep. Nippon Steel Technical Report No. 35, Nippon Steel, 32-42 (October 1987).

[11] P. R. Austin, Modelling of the blast furnace based on the multifluid concept with applications to advanced operations, Ph.D. thesis, Tohoku University, Japan (1997).

[12] Y. Ohno, M. Schneider, Effect of horizontal gas flow on liquid dropping flow in two dimensional packed bed, Tetsu-to-Hagane 74 (1988) 1923–1930.

[13] G. X. Wang, S. J. Chew, A. B. Yu, P. Zulli, Modeling the discontinuous liquid flow in a blast furnace, Metallurgical and Materials Transactions B 28B (1997) 333–342.

[14] G. X. Wang, D. Y. Liu, J. D. Litster, A. B. Yu, S. J. Chew, P. Zulli, Experimental and numerical simulation of discrete liquid flow in a packed bed, Chemical Engineering Science 52 (1997) 4013–4019.

[15] D. Y. Liu, G. X. Wang, J. D. Litster, Unsaturated liquid percolation flow through nonwetted packed beds, AIChE Journal 48 (2002) 953–962.

[16] Y. Eto, K. Takeda, S. Miyagawa, Experiments and simulation of the liquid flow in the dropping zone of a blast furnace, Iron and Steel Institute of Japan (ISIJ-International) 33 (1993) 681.

[17] J. Wang, R. Takahashi, J. Yagi, Simulation model of the gas-liquid flows in the packed bed, Tetsu-to-Hagane 77 (1991) 1585–1592.

[18] H. Takahashi, K. Kushima, T. Takeuchi, Two dimensional analysis of burden flow in blast furnace based on plasticity theory, Iron and Steel Institute of Japan (ISIJ-International) 29 (1989) 117–124.

[19] H. Takahashi, N. Komatsu, Cold model study on burden behaviour in the lower part of blast furnace, Iron and Steel Institute of Japan (ISIJ-International) 33 (1993) 655–663.

[20] M. Kuwabara, S. Takane, K. Sekido, I. Muchi, Mathmatical two-dimensional model of the blast furnace process, Tetsu-to-Hagane 77 (1991) 1593–1600.

[21] J. Chen, T. Akiyama, H. Nogami, J. Yagi, H. Takahashi, Modeling of solid flow in moving beds, Iron and Steel Institute of Japan (ISIJ-International) 33 (1993) 664–671.

[22] K. Takatani, T. Inada, Y. Ujisawa, 3-dimensional dynamic mathematical simulator of blast furnace, CAMP-Iron and Steel Institute of Japan 7 (1994) 50–53.

[23] Y. Kajiwara, S. J., Interraction between gas and liquid flow in a simulated blast furnace, J. Metall Trans. 10B.

[24] J. Yagi, Mathematical modeling of the flow of four fluids in a packed bed, Journal of Iron And Steel Research, International 33 (1993) 619–639.

[25] J. Castro, H. Nogami, J. Yagi, Transient mathematical model of blast furnace based on multi-fluid concept with application to high pci operation, Iron and Steel Institute of Japan (ISIJ-International) 40 (2000) 637–646.

[26] T. Sugiyama, A. Nakagawa, H. Shibaike, Analysis on liquid flow in the dripping zone of blast furnace, Tetsu-to-Hagane 75.

[27] S. J. Zhang, A. B. Yu, P. Zulli, B. Wright, U. Tuzun, Modelling of the solids flow in a blast furnace, Iron and Steel Institute of Japan (ISIJ-International) 38 (1998) 1311–1319.

[28] P. R. Austin, H. Nogami, J. Yagi, Computational investigation of scrap charging to the blast furnace, Journal of Iron And Steel Research, International 38.

[29] S. A. Zaimi, T. Akiyama, J. B. Guillot, J. Yagi, Validation of a blast furnace solid flow model using reliable 3-d experimental results, Iron and Steel Institute of Japan (ISIJ-International) 40 (2000) 332–341.

[30] J. A. Castro, H. Nogami, J. Yagi, Three-dimensional multi-phase mathematical modeling of the blast furnace based on the multifluid model, Journal of Iron And Steel Research, International 42.

[31] J. A. Castro, H. Nogami, J. Yagi, Numerical investigation of simultaneous injection of pulverized coal and natural gas with oxygen enrichment to the blast furnace, Journal of Iron And Steel Research, International 42.

[32] M. Chu, H. Nogami, J. Yagi, Numerical analysis on blast furnace performance under operation with top gas recycling and carbon composite agglomerates charging, Journal of Iron And Steel Research, International 44.

[33] M. Li, Y. Banda, T. Tsuge, Analysis of liquid distribution in non-uniformly packed trickle bed with single phase flow, Chemical Engineering Science 56.

[34] X. Wen, Y. Shu, K. Nandakumar, Profile in randomly packed beds from computer simulation, AIChE Journal 47.

[35] C.-s. Wang, M. Xiao-jing, Z. Shao-bo, X. Xing-guo, W. Wen-zhong, A new mathematical model for description of the liquid discrete flow within a packed bed, Journal of Iron And Steel Research, International 15 (2008) 16–23.

[36] C.-S. Wang, X.-J. Mu, A amthematical model capable of describing the liquid flow mainly in a blast furnace, International Journal of Minerals, Metallurgy and Materials 16 (2009) 505.

[37] S. J. Zhang, A. B. Yu, P. Zulli, B. Wright, P. Austin, Numerical simulation of solids flow in a blast furnace, Applied Mathematical Modelling 26 (2002) 141–154.

[38] H. Takahashi, M. Tanno, J. Katayama, Burden descending behavior with renewal of deadman in a two dimensional cold model of blast furnace, Iron and Steel Institute of Japan (ISIJ-International) 36 (11) (1996) 1354–1359.

[39] S. K. Das, A. Kumari, D. Bandopadhay, S. A. Akbar, G. K. Mondal, A mathematical model to characterize effects of liquid hold-up on bosh silicon transport in the dripping zone of a blast furnace, Appl. Math. Modelling 10.1016/j.apm.2011.02.045.

[40] N. Tsuchiya, M. Tokuda, M. Ohtani, The transfer of silica from the gas phase to molten iron in the blast furnace, Metallurgical Transactions B 7B (1976) 315–320.

[41] G. Wang, S. Chew, A. Yu, P. Zulli, Model study of liquid flow in blast furnace lower zone, Iron and Steel Institute of Japan (ISIJ-International) 37 (1997) 573–582.

[42] P. R. Austin, H. Nogami, J. Yagi, Analysis of actual blast furnace operations and evaluation of static liquid holdup effects by the four fluid model, Journal of Iron And Steel Research, International 38.

[43] H. Jin, S. Choi, J.-I. Yagi, J. Chung, Dripping liquid metal flow in the lower part of a blast furnace, Iron and Steel Institute of Japan (ISIJ-International) 50 (2010) 1023–1031.

[44] H. J. Jin, S. Choi, Numerical analysis of isothermal flow in lower part of blast furnace considering effect of cohesive zone, Ironmaking and Steelmaking 37 (2) (2010) 89–97.

[45] G. Danloy, J. Mignon, R. Munnix, G. Dauwels, L. Bonte, A blast furnace model to optimize the burden distribution, Tech. rep., Centre for Research in Metallurgy (CRM), Liége, Belgium, www.crm-eur.com (2009).

[46] A. Hamilius, M. Deroo, G. Monteyne, R. Bekaert, R. D'hondt, Blast furnace practice with stave- coolers and with a rotating chute for burden distribution, Ironmaking Proceedings, Chicago 37 (1978) 160–168.

[47] H. Nogami, M. Chu, J. Yagi, Numerical analysis on blast furnace performance with novel feed material by multi-dimensional simulator based on multi-fluid theory, Applied Mathematical Modelling 30 (2006) 1212–1228.

[48] R. e. a. Takahashi, Operation and simulation of pressurized shaft furnace for direct reduction, Ironmaking Proc. 43 (1984) 485–500.

[49] F. Fun, Rates and mechanisms of feo reduction from slags, Metall. Trans. 1 (1970) 2537–2541.

[50] O. Levenspiel, Chemical Reaction Engineering, Wiley, New York, 2nd Edition, 1976.

[51] E. Turkdogan, G. J. W. Kor, R. J. Fruehan, Iron Steelmaker 7 (1980) 268.

[52] H. Inoue, T. Terui, Y. Jeng, Y. Omori, M. Ohtani, Sio generation kinetics in the reaction of sic with carbon monoxide in the temperature range 1900-2000 c, Bull. Res. Inst. Min. Dressing Metall. 43 (1987) 43–52.

[53] B. Ozturk, R. J. Fruehan, Silicon transfer in blast furnace, Process Technol. Proc. 6 (1986) 959–966.

[54] A. B. Yu, G. X. Wang, S. J. Chew, P. Zulli, Modelling the gas-liquid flow in an ironmaking blast furnace, Progress in Computational Fluid Dynamics 4 (1) (2004) 29–38.

[55] G. S. Gupta, J. D. Litster, V. R. Rudolph, E. T. White, A cold model study of liquid flow in the blast furnace lower zone, in: 6th AusIIM Extractive Metallurgy Conference, Brisbane, 3-6 July 1994, 1994, pp. 295–301.

[56] G. Gupta, J. D. Litster, V. R. Rudolph, Model studies of liquid flow in the blast furnace lower zone, Journal of Iron And Steel Research, International 36 (1996) 32–39.

[57] G. Gupta, J. D. Litster, E. T. White, V. R. Rudolph, Nonwetting flow of a liquid through a packed bed with gas cross-flow, Metallurgical and Materials Transactions B 28B (1997) 597–604.

[58] P. Mackey, N. Warner, Studies in the vaporization of mercury in irrigated packed beds, Chemical Engineering Science 28 (1973) 2141–2154.

[59] N. Standish, Dynamic holdup in liquid metal irrigated packed beds, Chemical Engineering Science 23 (1968) 51–56.

[60] N. A. Warner, Liquid metal irrigation of a packed bed, Chemical Engineering Science 11 (1959) 149–160.

[61] D. Y. Liu, S. Wijeratne, J. D. Litster, Scand. J. Metall. 26 (1998) 79.

[62] J. Bridgewater, Granular Matter - An Interdisciplinary Apporach, Springer, 1994, Ch. Mixing and segregation mechanisms in particle flow, pp. 161–194.

[63] G. X. Wang, J. D. Litster, A. B. Yu, Simulation of gas-liquid flow in dripping zone of blast furnace involving impermeable fused layers, Iron and Steel Institute of Japan (ISIJ-International) 40 (7) (2000) 627–636.

[64] B. H. Xu, A. B. Yu, S. J. Chew, P. Zulli, Simulation of the gas-solid flow in a bed with lateral gas blasting, Powder Technol. 109 (2000) 14–27.

[65] S. J. Chew, P. Zulli, A. B. Yu, Modeling of liquid flow in the blast furnace, Journal of Iron And Steel Research, International 41 (2001) 1112.

[66] S. J. Chew, P. Zulli, A. B. Yu, Modelling of liquid flow in the blast furnace: Theoretical analysis of the effects of gas, liquid and packing properties, Iron and Steel Institute of Japan (ISIJ-International) 41 (2001) 1112–1121.

[67] S. J. Chew, P. Zulli, A. B. Yu, Modelling of liquid flow in the blast furnace: Application in a comprehensive blast furnace model, Iron and Steel Institute of Japan (ISIJ-International) 41 (2001) 1122–1130.

[68] V. Singh, G. S. Gupta, A discrete model for non-wetting liquid flow from a point source in a packed bed under the influence of gas flow, Chemical Engineering Science 61 (2006) 6855–6866.

[69] S. J. Chew, G. X. Wang, A. B. Yu, P. Zulli, Experimental study of liquid flow in the blast furnace cohesive zone, Ironmaking and Steelmaking 24 (1997) 392–400.

[70] P. Aussillous, D. Quere, Shapes of rolling liquid drops, Journal of Fluid Mechanics 512 (2004) 133–155.

[71] P. Dimitrakopoulos, J. J. L. Higdon, Displacement of fluid droplets from solid surfaces in low reynolds-number shear flows, Journal of Fluid Mechanics 336 (1997) 351–378.

[72] D. P. A., On the wind force needed to dislodge a drop adhered to a surface, Journal of Fluid Mechanics 196 (1988) 205–222.

[73] V. E. B. Dussan, On the stability of drops or bubbles to stick to non-horizontl surfaces of solids part 3: The influence of motion of surrounding fluid on dislodging drops, Journal of Fluid Mechanics 174 (1987) 381–397.

[74] V. E. B. Dussan, S. S. Davis, On motion of a fluid-fluid interfacealong a solid surface, Journal of Fluid Mechanics 65 (1974) 71–95.

[75] A. King, E. Tuck, Thin liquid layers supported by steady air-flow surface traction, Journal of Fluid Mechanics 251 (1993) 709–718.

[76] S. D. R. Wilson, The slow dripping of a viscous fluid, Journal of Fluid Mechanics 190 (1988) 561–570.

[77] K. Shibata, M. Shimizu, S. Inaba, R. Takahashi, J. Yagi, Pressure loss and hold-up powders for gas-powder two phase flow in packed beds, Iron and Steel Institute of Japan (ISIJ-International) 31 (1991) 434.

[78] J. Chen, H. Nogami, T. Akiyama, T. R., J. Yagi, Behavior of powders in a packed bed with lateral inlets, Iron and Steel Institute of Japan (ISIJ-International) 34 (1994) 133.

[79] P. Austin, H. Nogami, J. Yagi, A mathematical model of four phase motion and heat transfer in the blast furnace, Iron and Steel Institute of Japan (ISIJ-International) 37 (1997) 458–467.

[80] P. R. Austin, H. Nogami, J. Yagi, A mathematical model for blast furnace reaction analysis based on the four fluid model, Iron and Steel Institute of Japan (ISIJ-International) 37 (1997) 748–755.

[81] J. Castro, H. Nogami, J. Yagi, Numerical investigation of simultaneous injection of pulverized coal and natural gas with oxygen enrichment to the blast furnace, Iron and Steel Institute of Japan (ISIJ-International) 42 (2002) 1203 – 1211.

[82] H. Nogami, P. Austin, J. Yagi, K. Yamaguchi, Numerical investigation on effects of deadman structure and powder properties on gasand powder flows in lower part of blast furnace, Iron and Steel Institute of Japan (ISIJ-International) 44 (2004) 500–509.

[83] S. Pintowantoro, H. Nogami, J. Yagi, Numerical analysis of static holdup of fine particles in blast furnace, Iron and Steel Institute of Japan (ISIJ-International) 44 (2004) 304–309.

[84] N. Hidaka, T. Matsumoto, K. Kusakabe, S. Morooka, Transient accumulation behavior of fines in packed beds of pulverized coke particles, J. Chem. Eng. Jpn. 33 (2000) 152–159.

[85] X. F. Dong, D. Pinson, S. J. Zhang, A. B. Yu, P. Zulli, Gas-powder flow and powder accumulation in a packed bed i: Experimental study, Powder Technology 149 (2004) 1–9.

[86] M. Horio, Transport phenomena in the lower part of blast furnace, Iron and Steel Institute of Japan (ISIJ-International) 68.

[87] R. Jackson, The mechanics of fluidized beds: part i: the stability of computation of multiphase-flow phenomena with interphase slip,the state of uniform fluidisation, Trans. Inst. Chem. Eng. 41 (1963) 13–21.

[88] S. L. Soo, Multiphase Fluid Dynamics, Science Press, Beijing, 1990.

[89] S. K. Garg, J. W. Pritchett, Dynamics of gas-fluidized beds, J. Appl. Phys. 46 (1975) 4493–4500.

[90] D. Gidaspow, B. Ettehadie, Fluidization in two-dimensional beds with a jet: 2. hydrodynamic modeling, Ind. Eng. Chem. Fundam. 22 (1983) 193–201.

[91] J. A. M. Kuipers, W. Prins, W. P. M. Van Swaajj, Theoretical and experimental bubble formation at a single orifice in a two-dimensional gas-fluidized bed, Chem. Eng. Sci. 46 (1991) 2881–2894.

[92] A. Levy, Two-fluid approach for plug flow simulations in horizontal pneumatic conveying, Powder Technol. 112 (2000) 263–272.

[93] X. F. Dong, D. Pinson, S. J. Zhang, A. B. Yu, P. Zulli, Gas-powder flow in blast furnace with different shapes of cohesive zone, Applied Mathematical Modelling 30 (2006) 1293–1309.

[94] T. Sugiyama, Analysis on the powder movement and accumulation in the deadman and dripping zone of blast furnace by the experiment of the

powder-gas 2-phase flow through the parallel packed bed, CAMP-Iron and Steel Institute of Japan 9 (1996) 19–21.

[95] H. Yamaoka, Flow characteristics of gas and fine particles in a two-dimensional space of packed bed, Tetsu-to-Hagane 72 (1986) 2194 – 2201.

[96] M. Ichida, T. Nakayama, K. Tamura, H. Shiota, K. Araki, Y. Sugisaki, Behavior of fines in the blast furnace, Iron and Steel Institute of Japan (ISIJ-International) 32 (1992) 505–513.

[97] H. Yamaoka, Mechanisms of hanging caused by dust in a shaft furnace, Iron and Steel Institute of Japan (ISIJ-International) 31 (1991) 939–946.

[98] N. Hidaka, J. Iyama, T. Matsumoto, K. Kusakabe, S. Morooka, Entrainment of fine particles with upward gas flow in a packed bed of coarse particles, Powder Technology 95 (1998) 265–271.

[99] J. M. Steiler, R. Nicolle, P. Negro, M. Helleisen, N. Jusseau, B. Metz, C. Thirion, in: Proc. Ironmaking Conf., Vol. 50, ISS, Warrendale, PA, 1991, p. 715.

[100] X. F. Dong, A. B. Yu, J. M. Burgess, , D. Pinson, S. Chew, P. Zulli, Modelling of multiphase flow in ironmaking blast furnace, Ind. Eng. Chem. Res. 48 (2009) 214–226.

[101] R. Aoki, H. Nogami, H. Tsuge, T. Miura, T. Furukawa, Simulation of transport phenomena around the raceway zone in the blast furnace with and without pulverized coal injection, Iron and Steel Institute of Japan (ISIJ-International) 33 (1993) 646.

[102] S. Yuu, T. Umekage, T. Miyahara, Predicition of stable and unstable flows in blast furnace raceway using numerical simulation methods for gas and particles, Iron and Steel Institute of Japan (ISIJ-International) 45 (2005) 1406–1415.

[103] K. Takeda, F. C. Lockwood, Stochastic model of flow and dispersion of fine particles in a packed bed, Tetsu-to-Hagane 82 (1996) 492–497.

[104] K. Takeda, F. C. Lockwood, Integrated mathematical model of pulverised coal combustion in a blast furnace, Iron and Steel Institute of Japan (ISIJ-International) 37 (1997) 432–440.

[105] Y. Tsuji, T. Kawaguchi, T. Tanaka, Discrete particle simulation of two-dimensional fluidized bed, Powder Technol. 77 (79).

[106] B. P. B. Hoomans, J. A. M. Kuipers, W. J. Briels, W. P. M. Van Swaaij, Discrete particle simulation of bubble and slug formation in a two-dimensional gas-fluidized bed: A hard-sphere approach, Chem. Eng. Sci. 51.

[107] B. H. Xu, A. B. Yu, Numerical simulation of the gas-solid flow in a fluidized bed by combining discrete particle method with computational fluidd dynamics, Chemical Engineering Science 52 (1997) 2785.

[108] B. H. Xu, A. B. Yu, Comments on the paper numerical simulation of the gas-solid flow in a fluidized bed by combining discrete particle method with computational fluid dynamics-reply, Chemical Engineering Science 53 (1998) 2646–2647.

[109] H. P. Zhu, Z. Y. Zhou, R. Y. Yang, A. B. Yu, Discrete particle simulation of particulate systems: Theoretical developments, Chemical Engineering Science 62 (2007) 3378 – 3396.

[110] H. P. Zhu, Z. Y. Zhou, R. Y. Yang, A. B. Yu, Discrete particle simulation of particulate systems: A review of major applications and findings, Chemical Engineering Science 63 (2008) 5728–5770.

[111] A. B. Yu, B. H. Xu, Particle-scale modelling of gas-solid flow in fluidisation, Journal of Chemical Technology and Biotechnology 78 (2-3) (2003) 111–121.

[112] Y. Q. Feng, A. B. Yu, Assessment of model formulations in the discrete particle simulation of gas-solid flow, Industrial & Engineering Chemistry Research 43 (2004) 8378–8390.

[113] N. G. Deen, M. V. S. Annaland, M. A. Van Der Hoef, J. A. M. Kuipers, Review of discrete particle modeling of fluidized beds, Chemical Engineering Science 62 (2007) 28–44.

[114] K. W. Chu, A. B. Yu, Numerical simulation of complex particle-fluid flows, Powder Technology 179 (2008) 104–114.

[115] H. Zhou, G. Mo, J. Zhao, K. Cen, Dem-cfd simulation of the particle dispersion in a gas-solid two-phase flow for a fuel-rich/lean burner, Fuel 90 (2011) 1584–1590.

[116] K. W. Chu, B. Wang, A. B. Yu, A. Vince, G. D. Barnett, P. J. Barnett, Cfd-dem study of the effect of particle density distribution on the multiphase flow and performance of dense medium cyclone, Minerals Engineering 22 (2009) 893–909.

[117] P. N. Rowe, A. W. Nienow, Particle mixing and segregation in gas fluidized bedsa review, Powder Technology 15 (1976) 141–147.

[118] Y. Q. Feng, A. B. Yu, An analysis of the chaotic motion of particles of different sizes in a gas fluidized bed, Particuology 6 (2008) 549–556.

[119] K. D. Kafuia, C. Thornton, M. J. Adams, Discrete particle-continuum fluid modelling of gas-solid fluidised beds, Chemical Engineering Science 57 (2002) 2395–2410.

[120] K. Chattopadhyay, M. Isac, R. I. L. Guthrie, Applications of computational fluid dynamics (cfd) in iron- and steelmaking: Part 1, Ironmaking and Steelmaking 37 (8) (2010) 554–561.

[121] K. Chattopadhyay, M. Isac, R. I. L. Guthrie, Applications of computational fluid dynamics (cfd) in iron- and steelmaking: Part 2, Ironmaking and Steelmaking 37 (8) (2010) 562–569.

[122] X. Dong, A. Yu, J. ichiro Yagi, P. Zulli, Modelling of multiphase flow in a blast furnace: Recent developments and future work, ISIJ International 47 (11) (2007) 1553–1570, 3.

[123] A. B. Yu, Encyclopedea of Condensed Matter Physics, Elsevier, 2005, Ch. Powder Processing: Models and Simulations, pp. 401–414.

[124] E. Simsek, B. Brosch, S. Wirtz, V. Scherer, F. Krll, Numerical simulation of grate firing systems using a coupled cfd/discrete element method (dem), Powder Technology 193 (2009) 266–273.

[125] C. Y. Wang, Tramsport Phenomena in Porous Media, Oxford Pergamon, 1998, Ch. Modelling Multiphase Flow and Transport in Porous Media.

[126] Y. Kaneko, T. Shiojima, M. Horio, Dem simulation of fluidized beds for gas-phase olefin polymerization, Chemical Engineering Science 54 (1999) 5809.

[127] W. E. Ranz, W. R. Marshall, Evaporation from drops, Chemical Engineering Progress 48 (1952) 141.

[128] T. Swasdisevi, W. Tanthapanichakoon, T. Charinpanitkul, T. Kawaguchi, T. Tsuji, Prediction of gas-particle dynamics and heat transfer in a two-dimensional spouted bed, Advanced Powder Technology 16 (2005) 275.

[129] J. T. Li, D. J. Mason, A computational investigation of transient heat transfer in pneumatic transport of granular particles, Powder Technology 112 (2000) 273.

[130] J. T. Li, D. J. Mason, Application of the discrete element modelling in air drying of particulate solids, Drying Technology 20 (2002) 255.

[131] J. T. Li, D. J. Mason, A. S. Mujumdar, A numerical study of heat transfer mechanisms in gas-solids flows through pipes using a coupled cfd and dem model, Drying Technology 21 (2003) 1839.

[132] H. Zhou, G. Flamant, D. Gauthier, Dem-les of coal combustion in a bubbling fluidized bed. part i: gas-particle turbulent flow structure, Chemical Engineering Science 59 (2004) 4193.

[133] H. Zhou, G. Flamant, D. Gauthier, Dem-les simulation of coal combustion in a bubbling fluidized bed. part ii: coal combustion at the particle level, Chemical Engineering Science 59 (2004) 4205.

[134] X. Wang, F. Jiang, J. Lei, J. Wang, S. Wang, X. Xu, Y. Xiao, A revised drag force model and the application for the gas-solid flow in the high-density circulating fluidized bed, Applied Thermal Engineering 31 (14-15) (2011) 2254–2261.

[135] K. F. Malone, B. H. Xu, Particle-scale simulation of heat transfer in liquid-fluidised beds, Powder Technology 184 (2008) 189–204.

[136] J. Xiang, The effect of air on the packing structure of fine particles, Powder Technology 191 (2009) 280–293.

[137] B. Peters, Classification of combustion regimes in a packed bed based on the relevant time and length scales, Combustion and Flame 116 (1999) 297 – 301.

[138] B. Peters, Measurements and application of a discrete particle model (DPM) to simulate combustion of a packed bed of individual fuel particles, Combustion and Flame 131 (2002) 132–146.

[139] R. Mehrabian, S. Zahirovic, R. Scharler, I. Obernberger, S. Kleditzsch, S. Wirtz, A cfdmodel for thermal conversion of thermally thick biomass particles, Fuel Process. Technol. 95 (2012) 96–108.

[140] M. Gomez, Fast-solving thermally thick model of biomass particles embedded in a cfd code for the simulation of fixed-bed burners, Energy Convers. Manag. 105 (2015) 3044.

[141] J. Wiese, F. Wissing, D. Hhner, S. Wirtz, V. Scherer, U. Ley, H. Behr, Dem/cfd modelling of the fuel conversion in a pellet stove, Fuel Processing Technology 152 (2016) 223239.

[142] F. Sudbrock, H. Kruggel-Emden, S. Wirtz, V. Scherer, Convective drying of agitated silica gel and beech wood particle beds - experiments and transient dem-cfd simulations, Drying Technology 33 (2015) 15–16.

[143] V. Scherer, M. Mnnigmann, M. Berner, F. Sudbrock, Coupled dem-cfd simulation of drying wood chips in a rotary drum - baffle design and model reduction, Fuel 184 (2016) 896–904.

[144] F. Wissing, S. Wirtz, V. Scherer, Discrete element modelling of msw incineration on grate firing systems: Influence of waste properties, in: 41st International Technical Conference on Clean Coal and Fuel Systems, 05.-09. Juni 2016, Clearwater, Florida, USA, 2016.

[145] T. Oschmann, S. Wirtz, H. Kruggel-Emden, Investigation of heat transfer in packed/fluidized beds for spherical particles resolved by an implicit 3d finite difference approach, in: Partec 2016, 19.-21. April 2016, Nuremberg, Germany, 2016.

[146] B. Krause, B. Liedmann, J. Wiese, S. Wirtz, V. Scherer, Coupled three dimensional dem-cfd simulation of a lime shaft kiln - calcination, particle movement and gas phase flow field, Chemical Engineering Science 134 (2015) 834–849.

[147] C. Kloss, C. Goniva, A. Hager, S. Pirker, Models, algorithms and validation for opensource dem and cfd-dem, Progress in Computational Fluid Dynamics 12(2/3) (2012) 140–152.

[148] S. Radl, F. Krainer, T. Puffitsch, C. Kloss, Biot number effects on the local heat and mass transfer rate in fixed and fluidized beds, in: AIChE Meeting, Salt Lake City, 2015.

[149] J. Chen, J. Grace, M. Golriz, Heat transfer in fluidized beds: design methods, Powder Technol. 150 (2) (2005) 123–132.

[150] D. Baillis, J.-F. Sacadura, Thermal radiation properties of dispersed media: theoretical prediction and experimental characterization, J. Quant. Spectrosc. Radiat. Transf. 67 (5) (2000) 327–363.

[151] N. Decker, L. Glicksman, Heat transfer in large particle fluidized beds, Int. J. Heat Mass Transf. 26 (9) (1983) 1307–1320.

[152] D. Gloski, L. Glicksman, N. Decker, Thermal resistance at a surface in contact with fluidized bed particles, Int. J. Heat Mass Transf. 27 (4) (1984) 599–610.

[153] A. Goshayeshi, J. Welty, R. Adams, N. Alavizadeh, Local heat transfer coefficients for horizontal tube arrays in high-temperature large-particle fluidized beds: an experimental study, J. Heat Transf. 108 (4) (1986) 907–912.

[154] G. Toschkoff, S. Just, K. Knop, P. Kleinebudde, A. Funke, D. Djuric, G. Scharrer, J. Khinast, Modeling of an active tablet coating process, J. Pharm. Sci. 104 (12) (2015) 4082–4092.

[155] S. Amberger, S. Pirker, C. Kloss, Thermal radiation modeling using ray tracing in liggghts, in: 6th International Conference on Discrete Element Methods (DEM6), 2013.

[156] B. Peters, C. Bruch, T. Nussbaumer, Modelling of wood combustion under fixed bed conditions, Fuel 82 (6) (2003) 729–738.

[157] T. Fogber, S. Radl, A novel approach to calculate radiative thermal exchange in coupled particle simulations, Powder Technology 323 (2018) 24–44.

[158] W. Zhong, A. Yu, G. Zhou, J. Xie, H. Zhang, CFD simulation of dense particulate reaction system: Approaches, recent advances

and applications, Chemical Engineering Science 140 (2016) 16 – 43. doi:http://dx.doi.org/10.1016/j.ces.2015.09.035.
URL http://www.sciencedirect.com/science/article/pii/S0009250915006661

[159] http://openfoamwiki.net (February 2017).

[160] A. Faghri, Y. Zhang, Transport phenomena in multiphase systems, Academic Press, 2006.

[161] F. Hoffmann, Modelling Heteregeneous Reactions in Packed Beds and its Application to the Upper Shaft of a Blast Furnace, Phd. dissertation, University of Luxembourg (2014).

[162] A. Mahmoudi, PREDICTION OF HEAT-UP, DRYING AND GASIFICATION OF FIXED AND MOVING BEDS BY THE DISCRETE PARTICLE METHOD (DPM), Phd. dissertation, University of Luxembourg (2016).

[163] M. M., A Discrete Approach to Describe the Kinematics between Snow and a Tire Tread, Phd. dissertation, University of Luxembourg (2014).

[164] S. K., Assessment of implicit and explicit algorithms in numerical simulation of granular matter, Phd. dissertation, University of Luxembourg (2012).

[165] F. S. Mederos, J. Ancheyta, J. Chen, Review on criteria to ensure ideal behaviors in trickle-bed reactors, Applied Catalysis A: General 355 (12) (2009) 1 – 19. doi:10.1016/j.apcata.2008.11.018.

[166] S. Schwidder, K. Schnitzlein, A new model for the design and analysis of trickle bed reactors, Chemical Engineering Journal 207208 (2012) 758 – 765, 22nd International Symposium on Chemical Reaction Engineering (ISCRE 22). doi:10.1016/j.cej.2012.07.054.

[167] A. Atta, S. Roy, K. D. Nigam, Investigation of liquid maldistribution in trickle-bed reactors using porous media concept in {CFD}, Chemical Engineering Science 62 (24) (2007) 7033 – 7044, 8th International Conference on Gas-Liquid and Gas-Liquid-Solid Reactor Engineering. doi:10.1016/j.ces.2007.07.069.

[168] Y. Jiang, M. Khadilkar, M. Al-Dahhan, M. Dudukovic, {CFD} of multiphase flow in packed-bed reactors: I. k-fluid modeling issues, AIChE Journal 48 (4) (2002) 701–715. doi:10.1002/aic.690480406.

[169] P. R. Gunjal, M. N. Kashid, V. V. Ranade, R. V. Chaudhari, Hydrodynamics of trickle-bed reactors: experiments and cfd modeling, Industrial & Engineering Chemistry Research 44 (16) (2005) 6278–6294. arXiv:http://dx.doi.org/10.1021/ie0491037, doi:10.1021/ie0491037.
URL http://dx.doi.org/10.1021/ie0491037

[170] H. Xiao, J. Sun, Algorithms in a robust hybrid cfd-dem solver for particle-laden flows, Communications in Computational Physics 9 (02) (2011) 297–323.

[171] M. Baniasadi, B. Peters, Resolving multiphase flow through packed bed of solid particles using extended discrete element method with porosity calculation, Industrial & Engineering Chemistry Research 56 (41) (2017) 11996–12008. arXiv:http://dx.doi.org/10.1021/acs.iecr.7b02903, doi:10.1021/acs.iecr.7b02903.

[172] M. Baniasadi, B. Peters, Preliminary investigation on the capability of eXtended Discrete Element method for treating the dripping zone of a blast furnace, ISIJ International 48 (1).

[173] M. Baniasadi, M. Baniasadi, B. Peters, Coupled cfd-dem with heat and mass transfer to investigate the melting of a granular packed bed, Chemical Engineering Science 178 (2018) 136 – 145. doi:https://doi.org/10.1016/j.ces.2017.12.044.

[174] M. Baniasadi, M. Baniasadi, B. Peters, Application of the extended discrete element method (xdem) in the melting of a single particle, AIP Conference Proceedings 1863 (1) (2017) 180003. arXiv:http://aip.scitation.org/doi/pdf/10.1063/1.4992363, doi:10.1063/1.4992363.

[175] A. K. Shukla, R. Dmitry, O. Volkova, P. R. Scheller, B. Deo, Cold model investigations of melting of ice in a gas-stirred vessel, Metallurgical and Materials Transactions B 42 (1) (2011) 224–235. doi:10.1007/s11663-010-9442-9.

[176] E. Lassner, W.-D. Schubert, Tungsten: Properties, Chemistry, Technology of the Elements, Alloys, and Chemical Compounds, 1st Edition, Plenum Publishers, 1999.

[177] M. Weil, W.-D. Schubert, The Beautiful Colours of Tungsten Oxides, Tungsten (2013) 1–12.

[178] X.-W. Wu, J.-S. Luo, B.-Z. Lu, C.-H. Xie, Z.-M. Pi, M.-z. Hu, T. Xu, G.-G. Wu, Z.-M. Yu, D.-Q. Yi, Crystal Growth of Tungsten During Hydrogen Reduction of Tungsten Oxide at High Temperature, Transactions of Nonferrous Metals Society of China 19 (2009) 785–789.

[179] A. A. Estupinan Donoso, A Discrete-Continuous Approach to Model Powder Metallurgy Processes, Phd, University of Luxembourg (2016).

[180] S. Luidold, H. Antrekowitsch, Hydrogen as a Reducing Agent: State-of-the-art Science and Technology, J Miner Met & Mater Soc 2 (June) (2007) 20–27.

[181] R. Haubner, W.-D. Schubert, E. Lassner, M. Schreiner, Mechanism of Technical Reduction of Tungsten: Part 1 Literature Review, International Journal of Refractory Metals and Hard Materials 2 (September 1983) (1983) 108–115.

[182] A. A. A. Estupinan Donoso, B. Peters, XDEM Employed to Predict Reduction of Tungsten Oxide in a Dry Hydrogen Atmosphere, International Journal of Refractory Metals and Hard Materials 49 (March) (2015) 88–94. doi:10.1016/j.ijrmhm.2014.08.012.
URL http://authors.elsevier.com/a/1Qj9a{_}5-MTnPsJhttp://authors.elsevier.com/a/1Qj9a{%}7B{_}{%}7D5-MTnPsJ

[183] G. M. Barrow, Physical Chemistry, 6th Edition, McGraw-Hill, Boston, 1996.

[184] A. A. Estupinan Donoso, B. Peters, Predicting Tungsten Oxide Reduction with the Extended Discrete Element Method, Advances in Powder Metallurgy & Particulate Materials (2015) 02.35–02.48.

[185] M. Mohseni, Drying and conversion analysis of biomass by a dem-cfd coupling approach, Ph.D. thesis, University of Luxembourg (2017).

[186] A. Looi, K. Golonka, M. Rhodes, Drying kinetics of single porous particles in superheated steam under pressure, Chemical Engineering Journal 87 (2002) 329–338.

[187] M. Mohseni, B. Peters, Effects of particle size distribution on drying characteristics in a drum by xdem: A case study, Chemical Engineering Science 152 (2016) 689–689.

[188] G. Pozzetti, B. Peters, A multiscale DEM-VOF method for the simulation of three-phase flows, International Journal of Multiphase Flowdoi:10.1016/j.ijmultiphaseflow.2017.10.008.
URL http://www.sciencedirect.com/science/article/pii/S0301932216307327

[189] G. Pozzetti, B. Peters, On the choice of a phase interchange strategy for a multiscale DEM-VOF Method, AIP Conference Proceedings 1863.
URL http://orbilu.uni.lu/handle/10993/28863

[190] G. Pozzetti, B. Peters, Evaluating Erosion Patterns in an abrasive water jet cutting using XDEM, Advances in Powder Metallurgy & Particulate Materials (2017) 191–205.
URL http://hdl.handle.net/10993/31360

[191] B. Peters, G. Pozzetti, Flow characteristics of metallic powder grains for additive manufacturing, EPJ Web of Conferences 13001 (2017) 140.
URL http://hdl.handle.net/10993/31734

[192] K. Kleefsman, G. Fekken, A. Veldman, B. Iwanowski, B. Buchner, A volume-of-fluid based simulation method for wave impact problems, Journal of Computational Physics 206 (1) (2005) 363 – 393. doi:https://doi.org/10.1016/j.jcp.2004.12.007.
URL http://www.sciencedirect.com/science/article/pii/S0021999104005170

[193] S. Pope, Turbulent Flows, Cambridge Press.

[194] A. Toutant, E. Labourasse, O. Lebaigue, O. Simonin, {DNS} of the interaction between a deformable buoyant bubble and a spatially decaying turbulence: A priori tests for {LES} two-phase flow modelling, Computers & Fluids 37 (7) (2008) 877–886, special Issue of the "Turbulence and Interaction-TI2006" Conference. doi:10.1016/j.compfluid.2007.03.019.
URL http://www.sciencedirect.com/science/article/pii/S004579300700165X

[195] V. Armenio, U. Piomelli, V. Fiorotto, Effect of the subgrid scales on particle motion, Physics of Fluids 11 (10) (1999) 3030–3042. doi:10.1063/1.870162.
URL http://scitation.aip.org/content/aip/journal/pof2/11/10/10.1063/1.870162

[196] Q. Wang, K. D. Squires, Large eddy simulation of particle-laden turbulent channel flow, Physics of Fluids 8 (5) (1996) 1207–1223.

doi:10.1063/1.868911.
URL http://scitation.aip.org/content/aip/journal/pof2/8/5/10.1063/1.868911

[197] H. Zhou, G. Flamant, D. Gauthier, DEM-LES of coal combustion in a bubbling fluidized bed. Part I: gas-particle turbulent flow structure, Chemical Engineering Science 59 (20) (2004) 4193–4203. doi:10.1016/j.ces.2004.01.069.
URL http://www.sciencedirect.com/science/article/pii/S0009250904002933

[198] T. Burgener, D. Kadau, H. J. Herrmann, Simulation of particle mixing in turbulent channel flow due to intrinsic fluid velocity fluctuation, Physical Review E 83.